SUPERFLUID HYDROGEN IN NANOSCALE CONFINEMENT

by

Tokunbo P. Omiyinka

A thesis submitted in partial fulfillment of the requirements for the degree of

Master of Science

Department of Physics

University of Alberta

Abstract

Confinement is known to suppress order in condensed matter. This is well exemplified in phase transitions such as freezing, as well as the superfluid transition in liquid helium, which occur at lower temperatures in confinement than in the bulk. We provide in this thesis a demonstration of a physical setting in which the reverse takes place. Particularly, the enhancement of the superfluid response of parahydrogen confined to nanoscale size cavities is illustrated by means of first principle computer simulations. Prospects to stabilize and observe the long investigated but yet elusory bulk superfluid phase of parahydrogen in objectively designed porous media are discussed.

Preface

The entirety of this thesis constitute the original thesis research of Tokunbo Omiyinka, under the supervision of Professor Massimo Boninsegni.

Chapter 3 of this work has been published as: Tokunbo Omiyinka and Massimo Boninsegni, "Pair potentials and equation of state of solid *para*-hydrogen to megabar pressure", Physical Review B **88**, 024112 (2013).

Also, Chapter 4 has been published as: Tokunbo Omiyinka and Massimo Boninsegni, "Enhanced superfluid response of parahydrogen in nanoscale confinement", Physical review B **90**, 064511 (2014).

Acknowledgements

I am immensely grateful for having the opportunity to pursue my graduate studies at the University of Alberta. I am profoundly indebted to my supervisor, Prof. Massimo Boninsegni, who is responsible for every inch of success in my masters program and in making this thesis a reality. I am particularly thankful for your unrelenting dedication to constantly guide me through various learning curves, making it possible for me to achieve things I would have thought impossible. Thank you very much.

I also like to appreciate Prof. Kevin Beach whose support and recommendations were crucial to the start of my graduate studies. Many thanks to you.

To Sarah Derr, for your kindness in being always ready to guide and assist countless graduate students, including myself, I say a huge thank you.

To Gordon and Carol Buzikevich, your unrelenting support in every possible way, as well as your staying close to my family through our successes and challenges, are inestimable and worthy of unending thanks; thanks a great deal.

I am also very thankful to Kingsley Emelideme, Burkhard Ritter, Ebele Ezeokafor and Godfrey Obumneme for your enduring support in many ways. I also like to express my deep gratitude to many others whose varying support, encouragement and criticism contribute to the success of my masters degree.

To my most beloved parents (of blessed memory), Mr & Mrs. Akinposi and Adija Omiyinka, and my wonderful siblings (Bukola, Folake, Daniel, Goodness, Samuel and Testimony), I am full of thanks and inexpressible appreciation for

your relentless prayers and faith in me. I love you all. Uncle Muhammed Omisore, your prayers and best wishes go a long way in assisting me in my studies; thank you very much.

My dearest wife, *ayanfemi*, Oluwabukolami, your support, prayers, understanding, affection and love are sources of renewed life, strength and hope to me. I am most grateful to you beyond words. Many thanks to you as always.

I am also full of thanks for very helpful computing support from Westgrid and University of Alberta AICT.

God bless you all.

Table of Contents

1 INTRODUCTION **1**

2 PHYSICAL MODEL AND RESEARCH METHODOLOGY **8**

2.A The Many-body Hamiltonian 8

2.B The Continuous-space Worm Algorithm 11

2.B.1 Thermal Averages and Path Integration 11

2.B.2 Path Integral Monte Carlo and Quantum Statistics . . 13

2.B.3 Thermal Wavelength and Particle Permutations 15

2.B.4 Permutation Sampling In Conventional PIMC 16

2.B.5 Effective Permutation Sampling: The Worm Algorithm 17

2.B.6 Thermodynamic Estimators 19

3 PAIR POTENTIALS AND EQUATION OF STATE OF SOLID *PARA*-HYDROGEN TO MEGABAR PRESSURE **23**

3.A Introduction 24

3.B Model 29

3.C Calculation 32

3.D Results 34

3.E Conclusion 40

4 ENHANCEMENT OF SUPERFLUID RESPONSE OF PARAHYDROGEN IN NANOSCALE CONFINEMENT 42

4.A Introduction 42

4.B Results 43

4.B.1 Energetics 43

4.B.2 Structure of p-H_2 cluster in confinement 45

4.B.3 Enhanced superfluid response in cesium cavity 48

CONCLUSIONS 51

Bibliography 54

List of Tables

3.1 Time step extrapolation 33

3.2 Equilibrium density check on Moraldi potential 35

3.3 Comparison of pressures corresponding to different densities using various pair potentials 37

3.4 Kinetic energy per molecule at T=0 computed with SG, Buck and Moraldi potentials 40

List of Figures

2.1 Permutation sampling in conventional PIMC 16

2.2 A sample of the Configuration space G-sector 18

3.1 An example pair potential 26

3.2 The Moraldi pair potential: Our modification 32

3.3 Equation of state of p-H_2 from experiment and using different pair potentials 36

3.4 Comparison of the Pair correlation functions for Buck and Moraldi potentials 38

3.5 $T \to 0$ Kinetic energy per molecule computed with SG, Buck and Moraldi potentials 39

4.1 $T \to 0$ energy per hydrogen molecule inside Cs and Glass cavities of radius 10 Å 44

4.2 Radial density profile for 70 p-H_2 molecules in a Glass cavity at $T = 0.5$ K 45

4.3 Radial density profile for 32 p-H_2 molecules inside a Cs cavity, a Glass cavity, and in a free standing cluster, at $T = 1$ K . . . 47

4.4 Radial density profile for 30 p-H_2 molecules inside a Cs cavity, a Glass cavity, and in a free standing cluster, at $T = 0.5$ K . . 48

4.5 Probability of occurrence of permutation cycles 49
4.6 Momentum distribution 52

Chapter 1

INTRODUCTION

Superfluidity is the property of a substance capable of sustaining non-dissipative flow. It can occur in any of the three phases of aggregation of matter, including the solid, but is most easily observed and intuitively understood in a liquid. A superfluid liquid can remain in a state of persistent flow through a pipe, even in the absence of any pressure gradient, and several other manifestations of superfluid behavior, including rather spectacular ones such as the fountain effect, can be observed in any modern low temperature physics laboratory [1].

Helium is the only known *naturally occurring* substance that displays a superfluid phase. Under the pressure of its own vapour, helium condenses into a liquid at a temperature of 4.2 K [2]. It was simultaneously discovered by Kapitza [3], and Allen and Misener [4], that the liquid phase of its most abundant isotope (^{4}He) undergoes a second order transition to a superfluid phase at a temperature $T_\lambda = 2.17$ K. The less abundant isotope, ^{3}He, also turns superfluid, but at a much lower temperature, of the order of a few mK. A useful phenomenological model introduced by Tisza [5], which we shall

henceforth utilize, regards a superfluid under the transition temperature as a mixture of two fluids, a *normal* one, carrying entropy and subjected to dissipation like any ordinary fluid, and a *superfluid* component, capable of flowing without dissipation and not carrying any entropy. The fraction of the system in the superfluid phase is ρ_S, which is zero above T_λ and approaches unity as the temperature $T \to 0$, in a system featuring translational invariance (such as a liquid). Obviously, the normal fraction $\rho_N = 1 - \rho_S$.

Superfluidity is possibly the most interesting manifestation of quantum mechanics on a macroscopic scale. Decades of experimental and theoretical investigation have afforded considerable insight into the microscopic origin of superfluidity. In particular, it is now widely accepted [6] that, at least in three dimensions, superfluidity is intimately connected to a phenomenon called *Bose-Einstein Condensation* (BEC), which occurs in assemblies of indistinguishable particles of integer spin (Bosons). BEC consists of the occupation at low temperature of the same *single-particle* quantum-mechanical state by a *macrosopic* fraction of particles in the system. This explains, among other things, the difference in superfluid transition temperature between the two isotopes of helium, which arises from the fact that ^{3}He atoms have spin 1/2, and obey therefore Fermi statistics, i.e., they cannot undergo BEC by themselves. Thus, superfluidity in ^{3}He occurs through the formation of bound pairs of particles of opposite spin projections; such composite objects have spin zero, and can therefore act in some sense like bosons, undergoing BEC at a temperature of the order of the binding energy of the two mates of a pair. Indeed, such pairing mechanism is believed to underlie superfluidity in *all* Fermi systems, including electronic ones such as superconductors, which are themselves nothing but charged superfluids [1].

Significant progress toward the definitive understanding of superfluidity has been afforded by first principle computer simulations, based on the Path Integral formulation of quantum mechanics due to Feynman [7]. In particular, the Path Integral Monte Carlo method has proven instrumental in elucidating the subtle relationship between superfluidity and BEC [8], by showing unambiguously that superfluid ^{4}He is indeed a Bose-Einstein condensate, and that the superfluid response is underlain by cycles of exchange of indistinguishable particles (helium atoms) comprising a macroscopic fraction of all particles in the system (the same effect at the root of BEC).

Although in a sense one could argue that superfluidity is rather common, given the large number of elements that turn superconducting at low temperature, no other naturally occurring simple atomic or molecular substance has yet been found, other than ^{4}He, whose elementary constituents are Bose particles, that displays a superfluid phase. In the almost totality of other atomic or molecular systems, superfluidity is hindered by the large mass of the particles, as well as by the strong interactions among them, which causes the systems to crystallize at relatively high temperature, well above that at which BEC might take place. And, while as mentioned above there is nothing intrinsic preventing a *solid* from turning superfluid, it presently appears as if no naturally occurring superfluid solid exists [9].

An interesting, in many respects, "borderline" case is that of molecular hydrogen, specifically what is normally referred to as *parahydrogen* (p-H_2), which among naturally occurring substances is the closest possible candidate to feature superfluid character. Its elementary constituents are hydrogen diatomic molecules of spin zero (thus obeying Bose statistics) and of mass about one half that of a helium atom. The suggestion was first made in 1972 that a

fluid of p-H_2 molecules may undergo a superfluid transition at a temperature around 6 K [10]. However, the observation of this hypothetical superfluid has so far been made impossible by the fact that, unlike helium, p-H_2 solidifies at a temperature of 13.8 K, under the pressure of its own vapor. This results from the depth of the attractive well of the interaction between two p-H_2 molecules, about three times greater than that between two helium atoms, imparting to the system a strong propensity to crystallize, even in reduced dimensions [11].

The question thus naturally arises if one could suppress freezing, e.g., by *supercooling* the liquid phase, down to temperatures sufficiently low to allow the observation of superfluid transition. Reduction of dimensionality seems one possible avenue, as the freezing temperature of a substance is brought down by the lower coordination number; for example, the melting temperature of p-H_2 in two dimensions (2d) is almost half [12] of that in three dimensions (3d). However, theoretical studies of p-H_2 films adsorbed on diverse substrates [13, 14, 15] have not yielded any hint of possible superfluidity. A prediction that a finite superfluid response may arise in a (quasi) two dimensional film of p-H_2 intercalated within a crystalline grid of alkali metal atoms, originally made by Gordillo and Ceperley [16], has been disproven by successive, more accurate calculations [17].

One is then led to considering confinement as another avenue to stabilize a liquid phase of p-H_2 at low temperature [18, 19]; indeed, it is known experimentally that the freezing temperature of a fluid can be significantly lowered from its bulk value by confining it in a porous medium such as vycor glass [20, 21], which can be thought of as a random grid of interconnected cavities of average size $\sim$4 nm [22]. Notwithstanding, efforts to supercool liquid hydrogen by embedding it in a vycor matrix did not yield any evidence

of superfluid behaviour [23, 24]. Indeed, neutron scattering studies of p-H_2 in vycor glass at low temperature suggest that the system crystallizes in the pores, although with a different crystal structure [25], which is attributable to the pores' non-regular geometry, as well as to the strong attraction exerted on the p-H_2 molecules by the pore surface, where the crystal phase nucleates. It should also be mentioned that experimentally one observes the lowering of the superfluid transition temperature of liquid helium confined in vycor [26], to indicate that, while stabilizing the liquid phase, confinement has also the effect of suppressing superfluidity, and in general any ordered phase in condensed matter.

The questions remain open whether a different confining environment may make it possible to stabilize a superfluid phase of p-H_2, and how such a confining medium would be different from vycor. A hint comes from quantitative theoretical predictions that have been made [27, 28, 29] of superfluid behaviour in small p-H_2 clusters (thirty molecules or less), at temperatures of the order of a fraction of a K, of which some experimental confirmation has been obtained [30] (though not conclusively so [31]). The largest clusters that display a significant superfluid response at temperature $T \simeq 1$ K, have a size of approximately 1.6 nm, and comprise $N = 27$ p-H_2 molecules [32]; superfluidity is suppressed in clusters of greater size, owing to the increasing predominance of crystalline order which originates at the centre of the system. This suggests that a porous medium with cavities around 2 nm in size may prove suitable; such a medium ought to chose a weaker adsorbent than silica, so as to suppress crystallization of p-H_2 at the pore surface.

In order to investigate the above scenario and to gain insight in the effect of confinement on the superfluid response of p-H_2, we have carried out in

this thesis first principle computer simulations of a microscopic model of p-H_2 in spherical confinements of diameter between 10 and 20 Å. We utilized adsorption parameters that correspond to the interaction of p-H_2 with a cesium cavity substrate, as well as with a cavity surface in the ballpark of a silica substrate (glass). Cesium is one of the most weakly adsorbing substrates and it is known [33] that hydrogen fluid fails to wet it at low temperature, whereas glass is much more attractive to hydrogen molecules. This difference in adsorption between cesium and glass is clearly reflected in the observed structure of the p-H_2 molecules in the respective cavities. Generally, at the equilibrium filling in the cesium cavity the hydrogen molecules are less localised and both inter- and intra-shell quantum exchanges are enhanced as molecules tend to stay close to each other, significantly away from the cavity surface where crystallization occurs in stronger sorption media. For a cesium cavity of diameter 20 Å, we observed that the superfluid response of parahydrogen is greatly enhanced with respect to that which one would expect in a free cluster with the same number of molecules. This is a strong indication that a possible bulk superfluid phase of the parahydrogen might be observable in a suitably tailored porous medium, with cavities of that size and adsorption strength.

On the other hand, in a much more adsorbing glass cavity molecules sit more closely to the glass cavity surface, are highly localised and organize in rigid, concentric shells. These factors combine to suppress quantum exchanges and result in crystallization of the p-H_2 molecules within a glass cavity.

In the remainder of this thesis, we describe in detail the study that we have carried out and the main results. In the next section, we offer a description of the miscroscopic model utilized, as well as of the computational methodology that we have adopted.

In Chapter 3 of this thesis, we present results of a study that is propaedeutic to that of hydrogen in a cavity, and which we undertook before turning our attention to the main problem of our interest. Specifically, the reliability of a theoretical prediction on the behaviour of confined parahydrogen crucially hinges on an accurate description of the interaction between hydrogen molecules, over a wide range of pressures. This is because in confinement, hydrogen molecules experience varying degrees of compaction throughout the cavity, as the overall system is not homogeneous; thus, it is desirable to utilize a pair potential capable of reproducing accurately the equation of state of p-H_2 to high pressure. To this end, we considered a recently introduced pair potential, modified its repulsive core at short distance, and computed with it the low temperature equation of state of solid parahydrogen. We found excellent agreement of the experimentally measured equation of state for this system, up to megabar pressure.

The results of our simulations of p-H_2 in confinement as well as our observation of the enhancement of the superfluid response of these clusters in cesium cavity are detailed in Chapter 4. This thesis concludes with a discussion of the promising implications of our study for the realization of a stable bulk superfluid phase of p-H_2 in purposefully designed porous media.

Chapter 2

PHYSICAL MODEL AND RESEARCH METHODOLOGY

In this chapter, we present details of the physical model and computational approach adopted in our study of the superfluidity of *para*-hydrogen in nanoscale confinement.

2.A The Many-body Hamiltonian

Our system of interest consists of N p-H_2 molecules, represented as point particles of spin zero, enclosed in a spherical cavity of radius R, and is described by the following quantum-mechanical many-body Hamiltonian:

$$\hat{H} = -\lambda \sum_i \nabla_i^2 + \sum_{i<j} v(r_{ij}) + \sum_i V(r_i). \tag{2.1}$$

Here, the $\mathbf{r}_i$ are positions of all p-H_2 molecules, measured with respect to the centre of the cavity (made the origin), $r_{ij} \equiv |\mathbf{r}_i - \mathbf{r}_j|$ is the distance

between two p-H_2 molecules; $\lambda = \frac{\hbar^2}{2m} = 12.031$ KÅ^2, m being the mass of a p-H_2 molecule; v describes the interaction between any pair of p-H_2 molecules, while V describes the interaction of a p-H_2 molecule with the cavity. For v, which we regard as spherically symmetric, we use a modification of the well-known pair potential of Silvera and Goldman [34], which has been shown to afford an accurate reproduction of the experimental equation of state of solid p-H_2 up to megabar pressure [35]. Such accuracy for the equation of state is crucial for an inhomogeneous system like the one we are dealing with, as hydrogen molecules at different parts of the cavity certainly experience varying pressures, which could be very high close to the cavity surface; we discuss this in greater detail in Chapter 3. For V, assumed to be a function of only the distance of a molecule from the centre of the cavity, we take the following model potential [36]:

$$V(r) = 2D \left\{ \frac{b^9 F(x)}{(1-x^2)^9} - \frac{6b^3}{(1-x^2)^3} \right\}, \tag{2.2}$$

where $x \equiv r/R$, $F(x) = 5 + 45x^2 + 63x^4 + 15x^6$, $b \equiv (a/R)$, r is the distance of a p-H_2 molecule from the centre of the cavity, R is the fixed radius of the cavity, and a, D are two parameters that are adjusted to reproduce, as closely as allowed by such a relatively crude model, a specific particle-substrate interaction. Eq. (2.2) is the generalization to the case of a spherical cavity of the so called "3-9" potential, which describes the interaction of a particle with an infinite, planar substrate [36]. It is derived by considering the cavity enclosure as a uniform outward extension of the substrate, extending from the surface of the spherical cavity (enclosing the p-H_2 molecules) to infinity. An infinitesimal element of volume of the medium is then considered to interact with a molecule in the enclosed cavity via Lennard-Jones potential, also de-

scribed in Chapter 3. The three dimensional integral of such interactions with the particle (a p-H_2 molecule) located at a position $\mathbf{r}_i$ relative to the cavity's centre, results in $V(r_i)$ evaluated at $r_i = |\mathbf{r}_i|$ as presented in Eq. (2.2). The parameter D in Eq. (2.2) has the dimensions of an energy, and is essentially the depth of the attractive well of the potential experienced by the particle in the neighbourhood of the substrate, whereas a is a characteristic length, corresponding approximately to the distance of closest approach to the substrate, where the molecule begins to experience a strong repulsion.

It is worthwhile to clarify at this point that the model of the system that we employ here does contain some simplifications, primarily the assumption that the interaction between hydrogen molecules can be sufficiently accurately represented by a spherically symmetric pair potential, as well as the fact that a cavity is regarded as perfectly spherical and smooth. Even though one might expect significant alterations to the interaction between two p-H_2 molecules inside a nanoscale cavity, the weakness of the substrate seems to justify the continued use of a central pair potential as if the molecules interacted in vacuum. This is based on the expected minimum distance from the surface (over 3 Å) at which molecules will be sitting, as confirmed by our simulation results [37]. On the whole, regardless of its simplicity, such a model allows us to address the physical question we are exploring in this thesis, which is the effect of confinement on the superfluid response of p-H_2. Actually, equivalent or even simpler models (e.g., cavities with hard walls) have been adopted to investigate structure of ^{4}He and classical fluids in confinement [38, 39].

We have thus carried out a theoretical investigation of the low temperature ($T \to 0$) physical properties of the system described by Eqs. (2.1) and (2.2), by means of first principle computer simulations. We specifically utilized the

Worm Algorithm in the continuous space path integral representation. This well-established computational methodology enables one to compute thermodynamic properties of Bose systems at finite temperature, directly from the microscopic Hamiltonian, and it gives direct access to the energetic, structural and superfluid properties of the confined p-H_2 fluid, in practice with no uncontrolled approximations. It is therefore a well suited computational approach to address directly the physical issues of interest here.

2.B The Continuous-space Worm Algorithm

The Path Integral Monte Carlo (PIMC) technique is the most reliable computational method for studying superfluidity and Bose-Einstein condensation, as well as the connection between the two phenomena [40]. Our calculations exclusively utilize Path Integral Monte Carlo (PIMC) simulations based on the Continuous Space Worm Algorithm [41, 42]. The PIMC approach involves implementing the Feynman's Path Integral [43] formalism through a suitable Monte Carlo strategy. The PIMC scheme is accurate and has no adjustable parameter, taking the microscopic Hamiltonian as its only input. It also does not have any inherent bias, since no *a priori* assumption, e.g., a trial wave function, is needed. The methodology is numerically exact for Bose systems. For Fermi systems, not considered in this work, it is only approximate.

2.B.1 Thermal Averages and Path Integration

The thermal average of a physical observable, for an N-particle system described by Eq. (2.1) at temperature T, represented by an operator $\hat{\mathcal{O}}$, is

given by

$$\langle \hat{\mathcal{O}} \rangle = \frac{\mathrm{Tr}\,(\hat{\mathcal{O}}\hat{\rho})}{\mathrm{Tr}\,\hat{\rho}} = \frac{\int dR\, \mathcal{O}(R)\rho(R,R,\beta)}{\int dR\, \rho(R,R,\beta)} \tag{2.3}$$

where $R \equiv \mathbf{r}_1\, \mathbf{r}_2\, \ldots\, \mathbf{r}_N$, i.e, the positions of all the N particles in the N-particle configuration and $\beta = 1/(k_B T)$. Henceforth, we shall set $k_B = 1$. The many-body density matrix, $\rho(R, R, \beta)$, is given by

$$\rho(R,R,\beta) = \langle R|\mathrm{e}^{-\beta\hat{H}}|R\rangle \tag{2.4}$$

with $\hat{H}$ being the quantum-mechanical many-body Hamiltonian of Eq. (2.1) while the *partition function* is given by

$$Z = \int dR\, \rho(R,R,\beta)\,.$$

The many-body density matrix is not usually known and Eq. (2.3) is evaluated through the path integration procedure prescribed by R. P. Feynman in 1948. Accordingly, the partition function,

$$Z \propto \int \mathcal{D}R(u)\, \exp\left\{-\mathcal{S}[R(u)]\right\}\,. \tag{2.5}$$

The integration in Eq. (2.5) is performed over all possible continuous, β-periodic N-particle configuration paths $R(u)$.

$\mathcal{S}[R(u)]$ is the Euclidean action expressed as

$$\mathcal{S}[R(u)] = \int_0^\beta du\, \left\{ \sum_{i=1}^{N} \frac{m}{2\hbar^2} \left(\frac{d\mathbf{r}_i}{du}\right)^2 + \mathcal{V}(R(u)) \right\}\,, \tag{2.6}$$

having defined $u\hbar$ as the "*imaginary time*". $\mathcal{V} = \sum_{i<j} v(r_{ij}) + \sum_i V(r_i)$ as given

in Eq. (2.1). The Euclidean action is related to path balance between *kinetic* (path curvature) and *potential* energy, which depends on interactions, along the various paths. Generally, smooth, straight paths have higher probability while paths of high potential energy have lower probability.

2.B.2 Path Integral Monte Carlo and Quantum Statistics

The evaluation of the many-body density matrix, Eq. (2.4), the partition function, (2.5), and the thermal average, (2.1), is most suitably achieved through a well implemented Monte Carlo strategy. This involves employing the Metropolis Algorithm [44] to sample many-particle paths $R(u)$ through configuration space, based on a probability distribution proportional to $\exp[-\mathcal{S}(R(u))]$. Thermal expectation values, such as (2.1), are then calculated as *statistical* averages of the physical observable of interest along paths.

In the continuum, the action integral must be discretized. This leads inevitably to a time-step error that can however be made arbitrarily small. The discretization procedure is such that in place of the continuous many-particle path $R(u)$, one considers a discrete path $R(u) \equiv \{R_0, R_1, \ldots, R_{M-1}\}$ for a finite number of time slices M. The β-periodicity of the paths requires that $R_M = \mathcal{P}R_0$, where $\mathcal{P}$ denotes permutations of particle labels. Any choice of a finite M defines a corresponding time step, τ, such that $M\tau = \beta$. The simplest approximate action (due to path discretization) is given by

$$\mathcal{S}[R(u)] \approx \sum_{i}^{N} \sum_{l=0}^{M-1} \frac{m(\mathbf{r}_{il} - \mathbf{r}_{il+1})^2}{2\tau\hbar^2} + \tau \sum_{l=0}^{M-1} \mathcal{V}(R_l)\,. \tag{2.7}$$

(Indeed, were $\mathcal{V} = 0$ (no interaction between particles), any discretized form becomes exact as $M \to \infty$). The probability with which a discrete path $R(u)$ is sampled is then given by

$$\begin{aligned} P &\propto \exp\{-\mathcal{S}[R(u)]\} \\ &= \prod_{i=1}^{N} \prod_{l=0}^{M-1} \rho_\circ(\mathbf{r}_{il}, \mathbf{r}_{il+1}, \tau) \times \prod_{l=0}^{M-1} \mathrm{e}^{-U(R_l,\tau)}\,, \end{aligned} \tag{2.8}$$

where

$$\begin{aligned} \rho_\circ(\mathbf{r}, \mathbf{r}', \tau) &= \left(2\pi\hbar^2\tau/m\right)^{-d/2} \exp\left[-\frac{m(\mathbf{r}-\mathbf{r}')^2}{2\hbar^2\tau}\right] \\ &(d \text{ is the dimensionality of the configuration space}) \end{aligned} \tag{2.9}$$

is the density matrix of a *free particle*, and in the simplest approximation, Eq. (2.7),

$$U(R, \tau) = \tau \mathcal{V}(R)\,. \tag{2.10}$$

$U(R, \tau)$ will change in other approximations of the action, $\mathcal{S}$, so that the discrete action becomes exact in the limit $M \to \infty$.

Quantum statistics, i.e, particle indistinguishability, is effected in the above formalism by allowing $R(\beta{=}M\tau) = \mathcal{P}R(0)$, the permutation $\mathcal{P}$ implying that, while actual positions occupied by particles in $R(\beta)$ and $R(0)$ are the same, particles are allowed to trade place. This is a crucial ingredient, in Bose systems, to allow for the capturing of the physics of the system, such as superfluidity and Bose-Einstein condensation, underlain by quantum exchanges and particle indistinguishability [45].

Finally, the thermal expectation of a physical observable $\mathcal{O}$, given by Eq.

(2.3), is then evaluated as

$$\langle \hat{\mathcal{O}} \rangle \sim \frac{\sum_{paths} \eta^{\mathcal{P}} \mathcal{O}(R_{path})}{\sum_{paths} \eta^{\mathcal{P}}} \tag{2.11}$$

where $\mathcal{P}$ is the parity of the permutation associated with particle relabelling (exchange), $\mathcal{O}(R_{path})$ is the average value of $\mathcal{O}$ along a path and $\eta = +1$ for Bose , -1 for Fermi statistics.

The direct averaging over paths as expressed in Eq. (2.11) becomes exponentially intractable with increasing N for Fermi systems as the sum over paths comprises "*an alternating series of terms of opposite signs*", which very nearly cancel each other out, as is well communicated in Ref. [46]. This results in a very low "signal-to-noise" ratio, rendering the calculation not feasible in practice at low temperature.

For Bose systems, on the other hand, $\eta = +1$, and therefore no such problem arises. Because in this work we are only concerned with Bose systems, we shall make no further mention of the above difficulty, referred in the literature as "sign problem of quantum Monte Carlo".

2.B.3 Thermal Wavelength and Particle Permutations

Although in principle permutations of identical particles must be included, one can come up with a simple physical criteria to determine their importance in a given system at temperature T.

The characteristic "size" of a single particle path is measured by the thermal wavelength

$$\lambda_T = \frac{\hbar}{\sqrt{mT}}$$

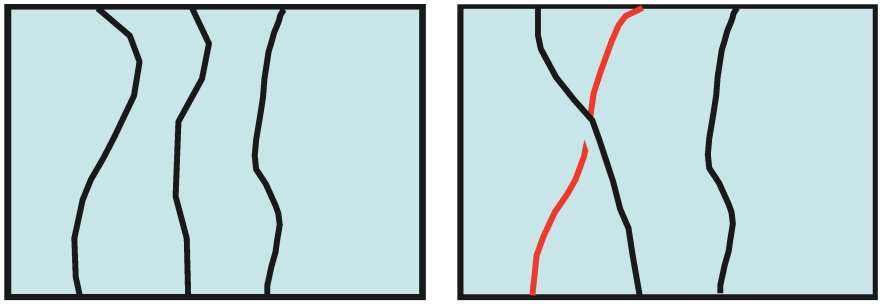

Figure 2.1: Permutation sampling in conventional PIMC

where m is the particle mass and T is the temperature. Permutations occur when λ_T is of the order of the mean interparticle distance. To put this in another way, assuming that $T_\circ$ is such that $\frac{\hbar}{\sqrt{mT_\circ}} \sim n^{-1/d}$, i.e, $T_\circ \sim \frac{\hbar^2 n^{2/d}}{m}$, where d is the dimensionality of the configuration space and n is the particle density, then:

- when $T > T_\circ$ permutations can be neglected as particles are typically distinguishable. Thus, one can assume $R(\beta) = R(0)$, or equivalently, $\mathcal{P} \equiv 1$, i.e., the identity permutation dominates.

- whereas when $T < T_\circ$ permutations become increasingly important for an accurate consideration of the quantum-mechanical problem involved.

2.B.4 Permutation Sampling In Conventional PIMC

Sampling of many-particle permutation paths is basic to an effective Monte Carlo implementation of the Path Integral formalism [47]. The path sampling procedure in the conventional implementation of PIMC, as in Ref. [48], is achieved through elementary moves that modify portions of single-particle paths. In particular, permutations are sampled by explicit construction of permutation cycles. As depicted in Fig. (2.1), this involves disconnecting the

world lines of individual particles in pairs and attempting to reconnect them together to achieve exchange cycles, while remaining in the diagonal sector of the configuration space. However, in the presence of any realistic interaction potential, typically possessing a repulsive and hard core, any such sampling of permutations is bound to have high likelihood of rejection and therefore becomes inefficient. Rejection occurs because the constructed trial path will almost always bring two particles within near vicinity of each other, i.e, the trial configuration will have high potential energy. In practice, efforts required to sample macroscopic permutation cycles scales exponentially with the system size. This challenge limits the number of particles for which the low temperature thermodynamics of a system can be effectively studied, making accurate extrapolation of results to the thermodynamic limit highly problematic, using the conventional PIMC implementation. The conventional PIMC implementation also does not allow for the simultaneous evaluation of diagonal and off-diagonal correlations, as its configuration space is locked in a canonical ensemble.

2.B.5 Effective Permutation Sampling: The Worm Algorithm

The Worm Algorithm completely resolves the issues mentioned above. A fundamental feature of the continuous-space worm algorithm is that it functions in an extended configurational space, including both closed world line configurations, referred to as the Z-sector, as well as configurations having one open world line (worm), known as the G-sector. A schematic view of the G-sector of the configuration space of the worm algorithm is seen in Fig. (2.2)

(from Ref. [49]). The Worm Algorithm simultaneously accumulate statistics for diagonal and off-diagonal correlations at no additional computational cost. All non-trivial topological modifications of the world lines that leads to long permutation cycles, as well as quantum exchanges, are intrinsically achieved through the G-sector. Closed world line configurations of the worm algorithm

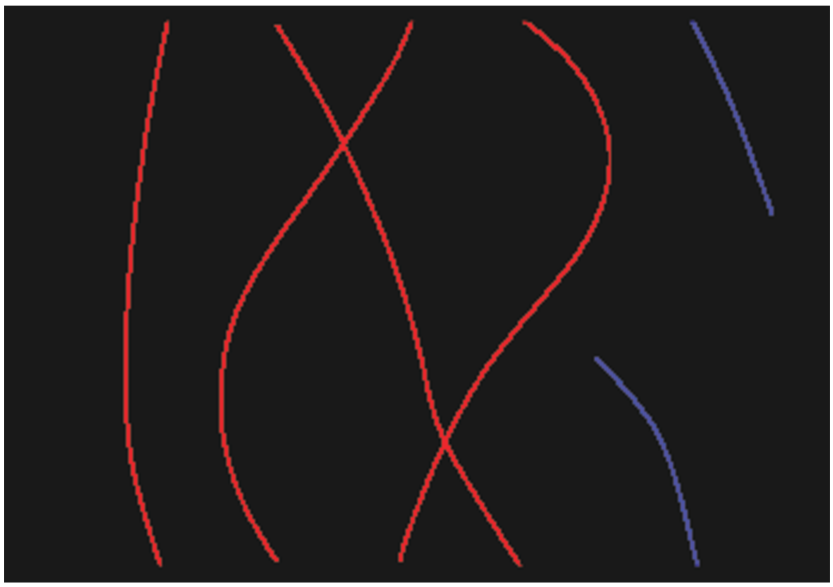

Figure 2.2: A sample of the Configuration space G-sector

.

contribute to the partition function, while configurations with an open world line, the *worm*, contribute to the one-particle *Matsubara Green function*. The *worm* is an open world line with two dangling ends which are referred to as Ira and Masha, denoted by $\mathcal{I}$ and $\mathcal{M}$ respectively in Fig. (2.2). The one-particle *Matsubara Green function* is expressed as

$$G(\mathbf{r}_1, \mathbf{r}_2, \tau) = -\langle \hat{\mathcal{T}}[\hat{\psi}(\mathbf{r}_2, \tau)\hat{\psi}^\dagger(\mathbf{r}_1, \tau = 0)]\rangle \,. \tag{2.12}$$

where $\hat{\psi}^\dagger$ and $\hat{\psi}$ are time-dependent Bose field operators, $\hat{\mathcal{T}}$ is the time ordering operator, $-\beta \leq \tau \leq \beta$. In the $\tau \to 0$ limit, the one-particle Matsubara

Green function reduces to the one-particle density matrix, $n(\mathbf{r}_2, \mathbf{r}_1)$, from which the momentum distribution is computed [50] directly in the continuous-space Worm Algorithm.

The Worm Algorithm accurately calculates various thermodynamic quantities of interest for large Bose systems in easily accessible computation time. These quantities include the energetics, structure, superfluid density, condensate fraction, one-body density matrix and momentum distribution. Another elegant feature of the Worm Algorithm is that it can be implemented in either a canonical or a grand-canonical ensemble (resulting from fluctuations of particle number through annihilation and creation of worms).

In our current application of the Worm Algorithm, the Z-sector configurations have a fixed number N of particles, while configurations in the G-sector are constrained to having $N-1$ particle world lines and a single worm.

Path Sampling In The Worm Algorithm

The Worm Algorithm automatically affords extensive sampling of intricate and non-trivial permutation cycles in both the Z- and G- sectors, while maintaining ergodicity regardless of the strongly repulsive core of microscopic interactions. This is readily achieved by its use of ergodic local path updates, in complementary pairs, that efficiently sample paths in its extended configuration space. For details, the reader is referred to Refs. [41, 42].

2.B.6 Thermodynamic Estimators

Having utilized the Worm Algorithm to obtain space-time configurations, of any quantum-mechanical system of interest, which are drawn from the ap-

propriate probability distribution (Eq. (2.8)), one becomes fully equipped to accurately compute the thermodynamic properties of the system, using appropriate thermodynamic estimators. For our study of superfluid hydrogen in nanoscale confinement, we computed the equilibrium total energy per *p*-H_2 molecule, $e(N)$, superfluid fraction, $\rho_S(T)$, radial density profile, $\rho(r)$ and the momentum distribution, $\bar{n}(\mathbf{k})$. The total energy per particle, useful for calculating the equation of state of the system, is obtained by summing its kinetic, $\langle K \rangle$ and potential, $\langle \mathcal{V} \rangle$, parts. These are calculated as described in Refs. [47, 51] as follows:

$$\langle K \rangle \approx \frac{3}{2\tau} - \frac{1}{4\lambda\tau^2} \left\langle (\mathbf{r}_l - \mathbf{r}_{l+1})^2 \right\rangle + \frac{\lambda\tau^2}{9} \left\langle \left(\nabla \mathcal{V}(\mathbf{R}_{2l}) \right)^2 \right\rangle , \tag{2.13}$$

where $\langle \cdots \rangle$ indicates the statistical average of the enclosed quantity, $(\mathbf{r}_l - \mathbf{r}_{l+1})^2$ is the square of the spatial separation of adjacent *beads* along a world line, while the gradient of the potential energy $\mathcal{V}$ is obtained with respect to the coordinate of one of the particles at an even time slice. For the potential energy per particle, the expression is

$$\langle \mathcal{V} \rangle \approx \frac{1}{N} \langle \mathcal{V}(\mathbf{R}_{2l-1}) \rangle . \tag{2.14}$$

Eqs. (2.13) and (2.14) both approach the exact results in the limit $M \to \infty$, $\tau \to 0$.

The superfluid fraction ($\rho_S(T)$), i.e., the fraction of a finite system that uncouples from a rotation that is induced externally, is obtained in the PIMC formalism as

$$\rho_S(T) = \frac{4m^2 T}{\hbar^2 I_c} \langle A^2 \rangle , \tag{2.15}$$

where A is the projection of the total area covered by the many-particle paths unto a perpendicular plane to one of the three symmetric rotation axes, I_c is the classical moment of inertia of the finite system (e.g p-H_2 cluster) and Eq. (2.15) is known as the *area estimator* [52].

As explained in Ref. [50], the momentum distribution is obtained from the one body density matrix $n(\mathbf{r}, \mathbf{r}')$ which is the $\tau \to 0$ limit of the Matsubara Green function, $G(\mathbf{r}, \mathbf{r}')$. For a system that is traslationally invariant, $n(\mathbf{r}, \mathbf{r}') \equiv n(\mathbf{r} - \mathbf{r}')$, and $\bar{n}(\mathbf{k})$ is given by the inverse transform

$$\bar{n}(\mathbf{k}) = \int d^3\mathbf{r}\, n(\mathbf{r}) \mathrm{e}^{-\imath \mathbf{k}\cdot\mathbf{r}} \,, \tag{2.16}$$

which for a system with spherically symmetric momentum distribution, i.e., $\bar{n}(\mathbf{k}) \equiv \bar{n}(k)$, becomes

$$\bar{n}(k) = \frac{4\pi}{k} \int_0^\infty dr\, r \sin kr\, n(r) \,, \tag{2.17}$$

having fixed the value of the one-body density matrix to unity at $r = 0$, hence the normalization

$$\frac{1}{(2\pi)^3} \int d^3\mathbf{k}\, \bar{n}(\mathbf{k}) = 1. \tag{2.18}$$

One then obtain the one body density matrix (OBDM) as described in Ref. [48].

We also estimate the standard error on our calculated expectation values. This is necessary as the expectation values are obtained as statistical averages using finite number ($\mathcal{M}$) of configurations ($\mathbf{X}$) and the mean of a physical observable over sample configurations will neccessary deviate from, and fluncTuate around, the true mean of the normal distribution that is reached in the

limit $\mathcal{M} \to \infty$. However, a straightforward estimate of the standard error on the mean using

$$\langle O \rangle_{\bar{\sigma}} = \sqrt{\frac{\sum_{k=1}^{\mathcal{M}} (O(\mathbf{X}_k) - \langle O \rangle)^2}{\mathcal{M}(\mathcal{M}-1)}}\,, \tag{2.19}$$

would underestimate the error, since the elements of our Markov chain are not completely independent and there exist an autocorrelation between the various $O(\mathbf{X}_k)$ given by [53]

$$\frac{\langle O_k O_{k+1} \rangle - \langle O_k \rangle^2}{\langle O_k^2 \rangle - \langle O_k \rangle^2}\,. \tag{2.20}$$

A reliable estimate of the standard error is obtained by reducing the autocorrelation between the quantities over which the average is sought. One way to do this would be to bin the entire $\mathcal{M}$ configurations into smaller configurations, average over each of the smaller configurations (thereby obtaining a set of averages that are less correlated than the initial set of averages over the original configurations set), and then finding the standard error on these new set of averages. We carry out a more rigorous estimation of the standard error using the blocking/bunching method (See Refs. [49, 54]).

Chapter 3

PAIR POTENTIALS AND EQUATION OF STATE OF SOLID *PARA*-HYDROGEN TO MEGABAR PRESSURE

An accurate $T = 0$ Path Integral Monte Carlo (PIMC) study of the system which we consider in this thesis, i.e., *para*-hydrogen clusters confined in spherical cavities, requires that one be able to reliably predict the equation of state of p-H_2 at non-trivial densities corresponding to very high pressures in the Gpa range. This is because the system is not homogeneous as in the hexagonally packed bulk structure, but the pressure exerted on a p-H_2 molecule may vary significantly throughout the cavity. Consequently, we carried out a detailed study of the accuracy of three different pair potentials in predicting the equation of state of solid p-H_2 to megabar pressure, covering the entire pressure range for which there is experimental data.

We compute by means of Quantum Monte Carlo simulations the equation of state of bulk solid p-H_2 extrapolated to zero temperature, up to a pressure of ∼2 Mbar. A comparison is made of the equation of state obtained by using the Silvera-Goldman (SG) and Buck [55] potentials, as well as a potential recently proposed by Moraldi [56], modified at short distances to include a repulsive core, missing in the originally proposed one. The Moraldi pair potential yields an equation of state in excellent agreement with experiment at megabar pressures, owing to its softer core, and is at least as accurate as the Buck at saturated vapor pressure.[1] This provides, to non-trivial pressures, a highly dependable description of the interaction between hydrogen molecules in a wide variety of configurations.

3.A Introduction

Hydrogen is known to be the simplest and most abundant element in the universe. Achieving predictive knowledge of its equation of state in a wide range of thermodynamic conditions has always been a worthwhile theoretical goal, owing to its relevance in a broad variety of physical systems, usually with possible technological applications [57, 58, 59], and also because it provides a cogent assessment of the most advanced computational many-body techniques.

The equation of state (EOS) of hydrogen, in essentially all phases of interest, is a fully quantum-mechanical problem. This is due to the fact the thermal wavelength of hydrogen is of the order of its mean inter-particle distance, causing the probability cloud (due to zero point motion) of individual

[1] A version of this chapter has been published as:
Tokunbo Omiyinka and Massimo Boninsegni. Physical Review B **88**, 024112 (2013).

molecules to significantly overlap with their neighbour's. Theoretical calculations broadly fall into two different categories; in *ab initio* studies, the mathematical model explicitly takes into account the ionic and electronic degrees of freedom, and their interaction via electrostatic Coulomb potential. Calculations are carried out within the framework of density functional theory (DFT) [60, 61, 62, 63, 64, 65] or Quantum Monte Carlo (QMC) [66, 67, 68, 69, 70, 71]. On the other hand, in molecular condensed phases, one often adopts the Born-Oppenheimer approximation, allowing one to regard individual hydrogen molecules as elementary particles, thus ignoring the electronic degrees of freedom. This approximation is mostly justified on the ground that the energy change pertaining to the first electronic excited state is of the order of 1 eV or $\sim$11588 K, which is order of magnitudes greater than the temperatures at which our studies are made (≤ 4 K), allowing us to consider the p-H_2 molecules as being effectively in their electronic ground state. Thus, one is able to describe the interaction between the molecules by means of a static potential, the simplest choice being that of a central pair potential.

In Fig. 3.1, we show the simplest example of a central pair potential, the Lennard-Jones potential, given by

$$V(r) = 4\epsilon \left[\left(\frac{\sigma}{r}\right)^{12} - \left(\frac{\sigma}{r}\right)^{6} \right]. \tag{3.1}$$

It shows the strong repulsion at short distances, characteristic of all microscopic pair potentials, due to *Pauli exclusion principle* preventing electrons of different molecules from spatially overlapping. Also evident are the weak *attraction* at long intermolecular distances ($r \gg \sigma$) owing to mutually induced electric dipoles, as well as a maximum well depth $\epsilon \sim 30$ K and core $\sigma \sim 3$ Å,

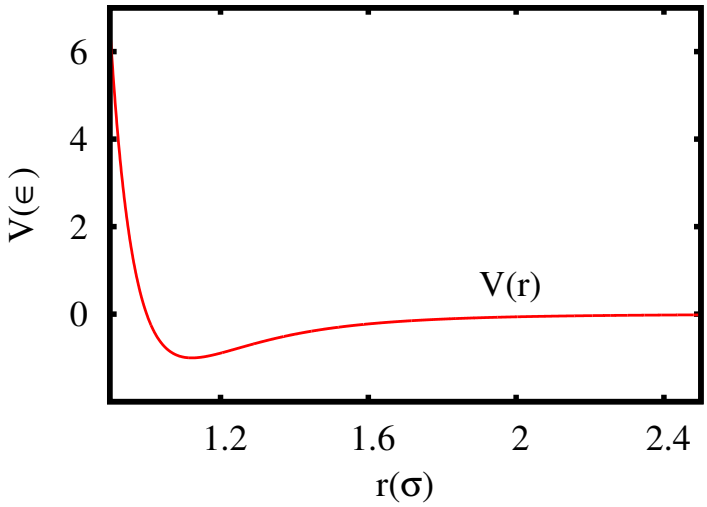

Figure 3.1: Lennard-Jones Potential

$[V(\sigma) = 0]$. More elaborate potentials are constructed in an attempt to provide better description of both the repulsive core and attractive tail. Notable examples for hydrogen are the Silvera-Goldman and Buck pair potentials.

Obviously, an approach based on a pair potential only dependent on the spatial separation between two molecules cannot describe any process involving electronic transfer, nor the energy contribution of interactions involving, say, triplets of molecules, nor any effect arising from the non-spherical features of the intermolecular interaction; the importance of all of these physical mechanisms generally increases with the thermodynamic pressure of the condensed phase under study. There are, however, distinct advantages to the use of static pairwise potentials, mainly, that it is typically computationally much faster and conceptually simpler than *ab initio* methods. Furthermore, if pair potentials are used, thermodynamic properties of molecular hydrogen

in condensed phase, and certainly in confinement, can be typically computed essentially without any uncontrolled approximation, e.g., by means of QMC simulations. Thus, it is desirable to develop pair potentials that afford reasonably accurate, quantitative description of the condensed phase of hydrogen in broad ranges of thermodynamic conditions. The Silvera-Goldman model pair potential is arguably the most commonly adopted, and has been shown [72] to afford a quantitative description of the low temperature equilibrium solid phase of p-H_2, whose superfluidity in nanoscale confinement we set out to examine. Another well known pair potential is the Buck [73, 74], which is very similar to the Silvera-Goldman, albeit with a slightly deeper attractive well. Both potentials yield an equation of state in reasonable agreement with experiment at moderate pressure ($\lesssim$25 kPa). At higher pressure, however, they become increasingly inaccurate, leading to an overestimation of the pressure due to the excessive "stiffness" of their repulsive core at short intermolecular separation (below $\sim$2.8 Å). This challenge is also present in the theoretical calculation of the equation of state of condensed helium at high pressure, based on pair potentials; in that context it is known that including three-body terms gives better agreement with the experimental equation of state, the overall effect being that of softening the repulsive core of the pairwise interaction [75, 76, 77].

Still, given the significant computational overhead involved in the inclusion of three-body terms, there remains the question of whether a modified effective pair potential could offer more satisfactory agreement of theory with experiment at high (e.g., megabar) pressure. To this aim Moraldi recently proposed a modified effective pair potential, with a softened repulsive core, designed to afford greater agreement between experiment and the theoretically predicted

values of the pressure as a function of the density in the low temperature limit ($T \to 0$). Results of perturbative calculations carried out in Ref. [56] show remarkable agreement with experimental data of the pressure computed with the new pair potential, in an extended range of density (up to 0.24 Å^{-3}, which corresponds to a pressure in the megabar range).

In this work, the $T = 0$ equation of state of solid p-H_2 is computed by means of first principle QMC simulations in a wider density range with respect to Ref. [56], namely, up to a density of 0.273 Å^{-3}, for a model of condensed p-H_2 based on three different pair potentials; our slightly modified version of the Moraldi potential (as shown in Fig. 3.2), the Silvera-Goldman, and the Buck. We provided a numerically accurate, non-perturbative check of the pressure computed in Ref. [56], and we offered a cogent comparison of the performance of the three potentials. We also compute the total and kinetic energy per molecule; the latter is experimentally measurable by means of neutron scattering, and is particularly sensitive to the detailed features of the repulsive core of the interaction [75].

We find that the recently proposed pair potential does indeed yield pressure estimates in much better agreement with experiment than the Silvera-Goldman and Buck potential, especially above 0.14 Å^{-3}. In fact, the agreement between the values of the pressure computed with the modified Moraldi potential and the ones measured experimentally remains excellent up to $\sim$180 GPa, the highest pressure for which experimental data are available for solid H_2. At the equilibrium density, i.e., zero pressure at $T = 0$, the Moraldi potential yields energy estimates comparable to those of the Silvera-Goldman. Kinetic energy estimates at high density computed with the Moraldi potential are significantly lower than those furnished by the Silvera-Goldman and Buck potentials, a fact

ascribable to the softer repulsive core of the Moraldi pair interaction. An experimental measurement of the kinetic energy will therefore provide additional important insights on whether the Moraldi potential not only yields an equation of state in quantitatively close agreement with experiment, but also affords a generally more accurate, quantitatively physical description of the system than the Silvera-Goldman or Buck model interactions.

We continue this chapter by presenting the particular microscopic model we adopt therein. We also illustrate the pair potentials we utilized, briefly highlighting the basic methodology underlying the calculation and offering relevant computational details in Sec. 3.C. In Sec. 3.D a thorough illustration of the results obtained in this work is provided. We finally provide a general discussion and conclusion to this chapter in Sec. 3.E.

3.B Model

Our system of interest in this chapter is modeled as an ensemble of N *para*-hydrogen molecules, regarded as point particles of spin zero, enclosed in a vessel of volume Ω, shaped as a parallelepiped, with periodic boundary conditions in all directions. The sides of the parallelepiped are chosen to fit a crystalline sample of solid *para*-hydrogen [hexagonal close packed (hcp) structure]. The quantum-mechanical many-body Hamiltonian is as follows:

$$\hat{H} = -\lambda \sum_{i=1}^{N} \nabla_i^2 + \sum_{i<j} v(r_{ij}) \tag{3.2}$$

Where, $\lambda = 12.031$ KÅ^2, while v is the potential describing the interaction between two p-H_2 molecules, only depending on their relative distance. As

we do make comparison between results from different pair-potentials in this work, we also provide here some basic details of all potentials used. The Silvera-Goldman (V_{SG}) and Buck (V_B) have the form

$$V(r) = V_{rep}(r) - V_{att}(r) f_C(r), \tag{3.3}$$

where $V_{rep}(r)$ describes the repulsion of two molecules at short distances, arising mainly from the Pauli exclusion principle, preventing the electronic clouds of different molecules from spatially overlapping, whereas $V_{att}(r)$ represents the long-range van der Waals attraction of mutually induced molecular electric dipoles. The purpose of the function $f_C(r)$ is to remove the divergence of $V_{att}(r)$ as $r \to 0$. For the Silvera-Goldman potential, V_{rep} is given by

$$V_{rep}(r) = \mathrm{e}^{-\alpha-\beta r-\lambda r^2}, \tag{3.4}$$

while V_{att} is given by

$$V_{att} = \frac{C_1}{r^6} + \frac{C_2}{r^8} - \frac{C_3}{r^9} + \frac{C_4}{r^{10}}. \tag{3.5}$$

Finally, $f_C(r)$ is given by

$$f_C(r) = \begin{cases} \mathrm{e}^{-\left(\frac{r_0}{r}-1\right)^2} & \text{if} \quad r < r_0, \\ 1 \quad \text{otherwise} \end{cases} . \tag{3.6}$$

The value of the constant parameters in the Silvera-Goldman expression are provided in Ref. [34]. In V_{att}, the term proportional to r^{-9} is the Axilrod-Teller estimate of the effective contribution of three-body interactions to the

potential, expected to be increasingly significant at high pressure and very low temperature ($T \to 0$). The expression for the Buck potential is similar to that of Silvera-Goldman, save the absence of the three-body term and the different values of its corresponding constants. As proposed in Ref. [56], the Moraldi potential is expressed as follows:

$$V_M(r) = V_{rep}(r) f_{rep}(r) - V_{att}(r) f_C(r), \tag{3.7}$$

where the functions V_{rep}, V_{att}, and f_C are the same as in the Silvera-Goldman potential; whereas f_{rep}, being of the same form as f_C, softens the repulsion at short distances contained in V_{rep}. It is given by

$$f_{rep} = \begin{cases} \exp\left(-a\left(\frac{r_0}{r} - 1\right)^n\right) & \text{if} \quad r < r_0, \\ 1 \quad \text{otherwise} \end{cases} . \tag{3.8}$$

where $a = 0.95$, $r_0 = 5.2$ a.u (1 a.u = 0.529 Å), and $n = 1.5$. The potential $V_M(r)$, as shown in Ref. [56], displays a much slower growth as $r \to 0$ than the Silvera-Goldman. In fact, the function $V_M(r)$ stops growing altogether at $r \sim r_0$ (see Fig. 3.2 below). This unphysical feature of $V_M(r)$ is of little consequences in calculations at low density, but must be corrected in order to prevent particles from "tunnelling" across the potential barrier and piling on top of one another, something we observed in computer simulations making use of $V_M(r)$ at densities for which the intermolecular distance is $\lesssim$2 Å. Thus, in this work we made use of the modified potential $U(r)$, defined as follows:

$$U(r) = V_M(r)\Theta(r - d) + \tilde{V}_{rep}\Theta(d - r), \tag{3.9}$$

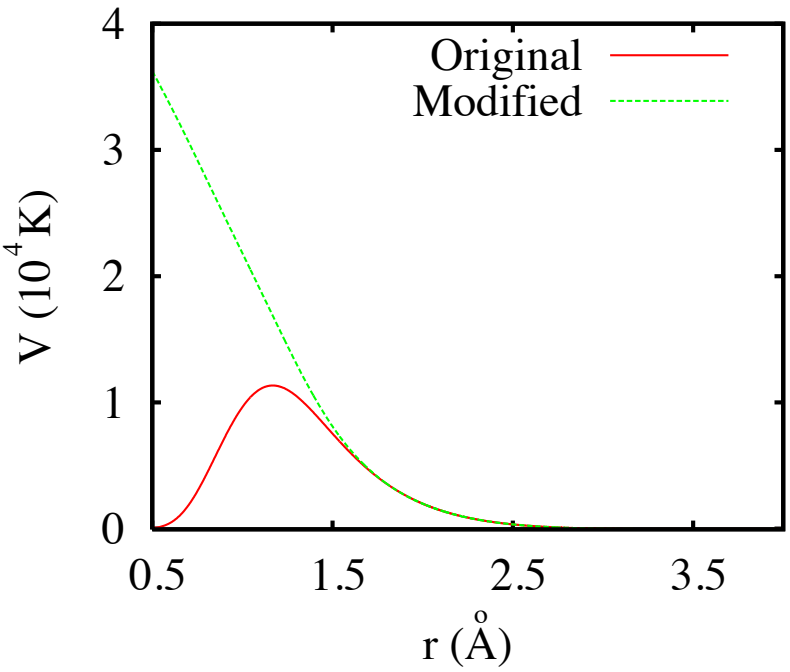

Figure 3.2: The Moraldi pair potential $V_M(r)$ as proposed in Ref. [56] (solid line) and the modified one $U(r)$ used in the present work (dashed line) [35]

where $d = 4$ a.u (i.e. 2.1167 Å), $\Theta(x)$ is the Heaviside function, and $\tilde{V}_{rep}(r)$ has the same form of V_{rep}, but the two parameters (usually referred to as α and β) upon which it depends are adjusted to match $V_M(r)$ and its first derivative at $r = d$. This modified potential, utilized in our simulations, is shown alongside $V_M(r)$ in Fig. 3.2. It lacks the unphysical feature of $V_M(r)$ at short distances discussed above; indeed, it increases monotonically as $r \to 0$.

3.C Calculation

The $T = 0$ (ground state) equation of state of solid *para*-hydrogen, modelled by the many-body Hamiltonian (3.2) with the three different potentials

V_{SG}, V_B and U described above, was computed by means of numerical QMC simulations based on the Continuous-Space Worm Algorithm. Specifically, we computed the pressure P as a function of the density ρ, in the interval $0.0763\,\text{Å}^{-3} \leq \rho \leq 0.273\,\text{Å}^{-3}$, for a finite system comprising $N = 216$ molecules. In order to provide ground state estimates, we perform simulations at different low temperatures and extrapolate the results to $T = 0$. We generally find that results obtained at $T = 4$ K are indistinguishable from the extrapolated ones, within our quoted statistical uncertainties. We employ the standard virial estimator [78] for pressure, and estimate the contribution from particles lying outside the main simulation cell by radially integrating the quantity $r(dV/dr)$, approximating the pair correlation function $g(r)$ to 1 (we do the same for the potential energy) [79].

Density	Time step	Energy	Pressure
0.076	39×10^{-4}	1.40×10^{3}	5.75×10^{4}
0.076	20×10^{-4}	1.50×10^{3}	5.79×10^{4}
0.076	10×10^{-4}	1.53×10^{3}	5.92×10^{4}
0.076	5.0×10^{-4}	1.53×10^{3}	5.92×10^{4}

Table 3.1: Time step extrapolation ($\tau \to 0$) for Pressure (in bars) and Energy in (K) calculated at 0.076 Å^{-3}) in the $T \to 0$ limit, using Silvera-Goldman potential. Combined statistical and systematic errors affecting our QMC simulations are estimated to be of the order of 0.1% or less of the quoted values.

We obtain our QMC results, as presented herein, with a time step $\tau = 5 \times 10^{-4}$ K^{-1}. Indeed, we observed that the estimates yielded by such a choice of time step coincide with those extrapolated to $\tau = 0$, within statistical uncertainties, as illustrated in Table 3.1. It is worth emphasizing that, in principle, *para*-hydrogen molecules must be regarded as indistinguishable particles of spin

zero, and thus obeying Bose statistics. The Worm Algorithm explicitly allows for permutation of identical particles, and quantum-mechanical exchanges can be important in p-H_2, in specific situations. They are in fact known to underlie superfluidity at low temperature in small clusters (< 30 molecules) [80], and their effect is measurable in the momentum distribution of liquid *para*-hydrogen near melting [81]. However, in the solid phase, in the range of density explored here, exchanges are practically absent, i.e., particles can be regarded for practical purposes as distinguishable.

3.D Results

While our work in this chapter is mainly aimed at the equation of state of solid p-H_2 at relatively high (megabar) pressure, we start the discussion of our results by illustrating the results of QMC simulations at the saturation density $\rho_\circ = 0.0261$ Å^{-3}. Specifically, we compare the pressure and energy estimates yielded by the Moraldi potential (modified as explained above), which was not purposefully designed to describe the low-density equilibrium phase, to those yielded by the Silvera-Goldman and Buck potentials, as well as to experimental data. We make such a comparison in order to ascertain whether the softening of the Silvera-Goldman repulsive core, which is at the basis of the Moraldi potential, might worsen the agreement with experiment at low density while possibly improving it in the megabar pressure range. Table 3.2 shows numerical estimates of the ground state energy per molecule for solid *para*-hydrogen at saturation density. The estimates here, obtained by extrapolating all the way down to $T = 0$ results obtained in the range 1 K $\leq T \leq$ 4 K, are in agreement with those given in Ref. [72] using ground state diffusion

	This work	Ref. [72]
Moraldi	-88.5(2)	
Silvera-Goldman	-88.1(1)	-87.90(2)
Buck	-93.8(1)	-93.87(2)

Table 3.2: Ground state energy per molecule (in K) for solid parahydrogen in the *hcp* phase at the saturation density $\rho_\circ = 0.0261$ Å^{-3}, computed in this work and in Ref. [72] for various intermolecular potentials. Statistical errors, in parentheses, are on the last digit.

Monte Carlo (DMC) simulations. Experimentally, the ground state energy per molecule has been inferred by various methods, and the agreement between the various predictions [82, 83, 84, 85] is not perfect; quoted values range from -89.9 K of Ref. [84] to -93.5 K of Refs. [83] and [85]. It is obvious from the data reported in Table 3.2 that the Moraldi potential affords an accuracy comparable to that of the other two potentials.

We make a comparison in Fig. 3.3 of our computed values of the pressure (with the three pair-potentials) for hcp *para*-hydrogen in the $T \to 0$ limit, in a density range up to 0.273 Å^{-3}, which corresponds to a pressure of about 1.8 Mbar. Also included for comparison is a fit to the most recent [86] compilation of experimental (x-ray) measurements [87, 88, 89] of the equation of state obtained with the Vinet equation of state [90],

$$P = \frac{3K_\circ(1-d)}{d^2}\exp\left[\frac{3}{2}(K'_\circ - 1)(1-d)\right], \tag{3.10}$$

where $d \equiv (\rho_\circ/\rho)^{1/3}$, with parameters $K_\circ = 0.20(1)$ GPa and $K'_\circ = 6.84(7)$. We also report the computed values of the pressure in Table 3.3.

The agreement between the experimental values of the pressure and those obtained by simulation using the Moraldi potential is excellent, considering the

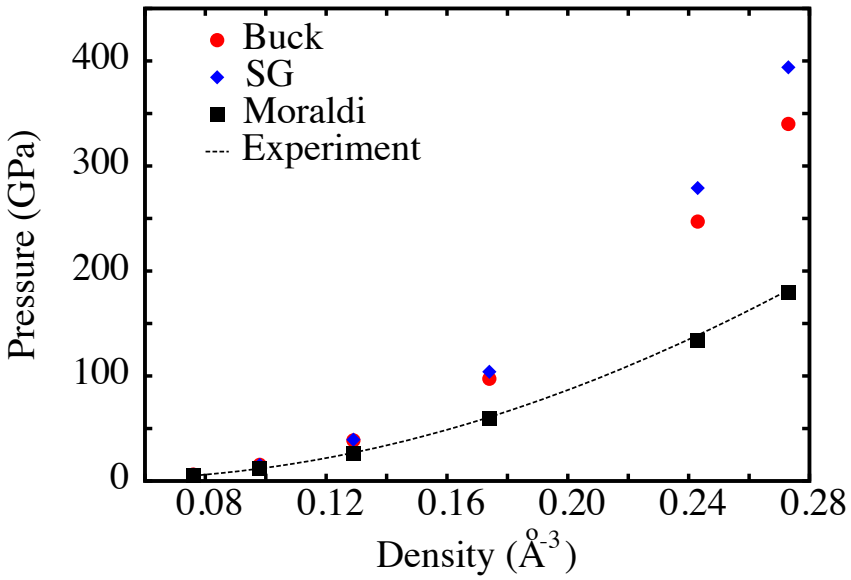

Figure 3.3: Equation of state of solid parahydrogen at T=0, computed by Quantum Monte Carlo simulations using the Silvera-Goldman (diamonds), Buck (circles) and Moraldi (boxes) pair potentials. Dashed line represents a fit to experimental data from Ref. [86] obtained with the Vinet equation of state (see text). Combined statistical and systematic errors affecting our computed pressures are at the most of the order of 0.1% of the pressure.

relatively simple form of the pair potential itself. At the highest compaction examined here, i.e., 0.273 Å^{-3}, the Silvera-Goldman potential overestimate the pressure by over a factor of 2. The Buck potential does only slightly better than the Silvera-Goldman. The lower values of pressure yielded by the Moraldi potential are a direct consequence of its softer repulsive core. It is noteworthy that the values in Table 3.3 agree quantitatively with those obtained by Moraldi in Ref. [56], using a perturbative calculation. Perhaps a more significant fact is the excellent agreement with experiment obtained using the *modified* Moraldi potential even above 110 GPa, i.e., a compression at which solid hydrogen undergoes an orientational phase transition [91]. One

Density	Moraldi	Buck	SG
0.076	5.11×10^4	6.09×10^4	5.92×10^4
0.098	1.17×10^5	1.54×10^5	1.52×10^5
0.129	2.61×10^5	3.87×10^5	3.93×10^5
0.174	5.93×10^5	9.74×10^5	1.04×10^6
0.243	1.34×10^6	2.47×10^6	2.79×10^6
0.273	1.80×10^6	3.40×10^6	3.94×10^6

Table 3.3: Pressure (in bars) calculated for different densities (in Å^{-3}) in the $T \to 0$ limit, using Buck, Silvera-Goldman and Moraldi potentials. Combined statistical and systematic errors affecting our QMC simulations are estimated to be of the order of 0.1% or less of the quoted values.

would anticipate that the approximation of a spherically symmetric potential, for the interaction between two p-H_2 molecules, would break down quickly as the system assumes the orientationally ordered phase.

The fact that the Moraldi potential is not as stiff as the Silvera-Goldman or Buck potentials at short distances is also reflected on the predicted structural properties of the crystal. Specifically, the local environment experienced by a single molecule is captured by the static structure factor, which of course can be probed by x-ray diffraction. Its Fourier inverse, the pair correlation function $g(r)$, is easily accessible by simulation. Results for two different densities are shown in Fig. 3.4, where the pair correlation functions computed for the Buck and Moraldi potentials are juxtaposed. The SG and Buck potentials yield similar results for this quantity [the main peak of the $g(r)$ being $\sim$10% higher with the SG potential, at the higher density]. While at the lower density, which corresponds to a pressure around 5 kbar, the pair correlation functions yielded by the two potentials are comparable, at the higher density (which corresponds to a pressure close to 1 Mbar), there is a clear difference between

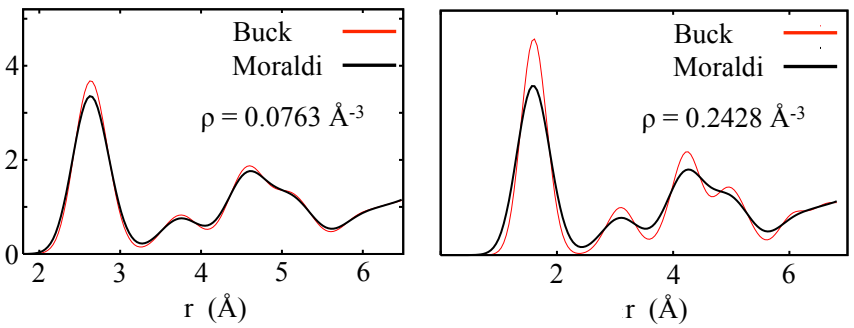

Figure 3.4: Pair correlation function $g(r)$ for hcp *para*-hydrogen at T=4 K, computed by simulation at the two densities ρ=0.0763 Å^{-3} and ρ=0.2428 Å^{-3}, with the Moraldi and Buck potentials. The results for the Silvera-Goldman potential are similar to those for the Buck.

the two results. In particular, the pair correlation function computed with the Buck potential has considerably higher peaks and generally much sharper features and an altogether more classical structure compared to that obtained with the softer Moraldi potential, which is smoother, and displays a markedly more quantum-mechanical character.

While the improvement afforded by the Moraldi potential on the calculation of the equation of state of p-H_2 is remarkably peculiar, especially putting the relatively wide spectrum of pressure for which it is observed into consideration, some care should be applied if a holistic evaluation is desired of the microscopic physical description yielded by a given pair potential. Quite possibly, one could obtain (by means of an effective pair potential) an equation of state in close concordance with experiment, but at the cost of worsening the reliability for other quantities.

More so, the kinetic energy per particle is especially sensitive to the detailed shape of the repulsive core of the intermolecular potential at short distances (see, for instance, the discussion in Ref. [75]), and it can be measured exper-

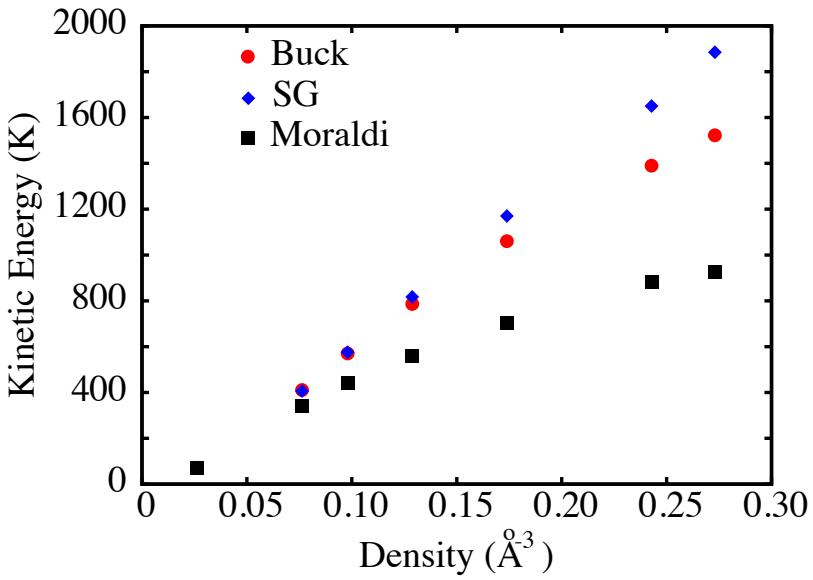

Figure 3.5: Kinetic energies per molecule at T=0, computed by simulations at different densities for the three potentials considered here.

imentally by neutron scattering, as the second moment of the single-particle momentum distribution [92]. Thus a cogent test of the relative accuracy of this potential could be offered by the measurements of the kinetic energy per particle, for which we provide ground state estimates as well, for all three potentials we examined here. The results are displayed in Fig. 3.5 and elaborated in Table 3.4.

At the saturation density, $\rho_\circ = 0.0261$ Å^{-3}, all potentials yield practically the same kinetic energy per molecule, whereas at higher density the softer core of the Moraldi potential leads to a considerably lower kinetic energy, especially at the highest compression. It is interesting to note however, that the contribution of the kinetic energy to pressure is minimal in comparison to that arising from intermolecular interactions. A close comparison of the estimates obtained herein with those reported in Ref. [56] shows that the

Density	Moraldi	SG	Buck	Ref. [56]
0.0261	69	70	71	
0.0763	341	406	411	405
0.0980	440	576	570	531
0.1288	558	817	786	678
0.1739	701	1170	1060	834
0.2428	872	1650	1390	914
0.2730	927	1855	1523	

Table 3.4: Kinetic energy per molecule (in K) in the $T \to 0$ limit, at various densities (in Å^{-3}), obtained using each of the three pair potentials considered in this work in the QMC simulation. Combined statistical and systematic errors affecting our results are estimated at one percent or less of the quoted values. Also reported are the estimates from Ref. [56], in the rightmost column.

perturbative approach slightly overestimates, but otherwise provide reasonably accurate results for the problem of interest.

3.E Conclusion

In this chapter, we have carried out a numerical analysis of an intermolecular potential proposed by Moraldi, intended to reproduce the experimental equation of state of solid *para*-hydrogen at low temperature, up to a pressure of $\sim$2 Mbar. The potential utilized here is a modification of the one proposed in Ref. [56], to which a repulsive core has been added at short distances, to prevent unphysical behaviour at the highest densities considered. This potential possesses an appreciably softer core than the Silvera-Goldman and Buck potentials, leading to improved quantum effects and reduced values of the pressure. We have performed Quantum Monte Carlo simulations of hcp *para*-hydrogen at different densities and compared the estimates yielded by

this potential with those of the Silvera-Goldman and Buck potentials, for the pressure and for the kinetic energy per molecule. We have also compared the numerical results to the most recent experimental equation of state, and found that this potential yields excellent agreement with experiment, agreement that we found extend all the way down to low density (saturation). We also provide estimates for the kinetic energy per molecule which is experimentally obtainable by neutron diffraction. Thus, we set out for our study of *para*-hydrogen in nanoscale confinement, equipped with a pair potential, whose description of the microscopic interaction between p-H_2 molecules is more reliably accurate, from zero to megabar pressures, than other well known potentials based on the excellent agreement with experimental data of the equation of state it furnishes.

Chapter 4

ENHANCEMENT OF SUPERFLUID RESPONSE OF PARAHYDROGEN IN NANOSCALE CONFINEMENT

4.A Introduction

In this chapter, we expound the results of our simulation of p-H_2 clusters in nanoscale cavities, especially our observation of the significant enhancement of the superfluidity of these clusters with respect to their free counterparts [1].

We illustrate below two sets of simulation results, both obtained by setting

[1] A version of this chapter has been published as:
Tokunbo Omiyinka and Massimo Boninsegni, Physical Review B **90**, 064511 (2014).

the cavity radius R to 10 Å, but with two distinct choices of parameters D and a (as in Chapter 2), corresponding to very different adsorption strengths. The first choice, which we label hereafter with Cs, has $D = 37.82$ K and a =3.88 Å; these are the recommended [93] values to describe the interaction of a p-H_2 molecule with a Cs substrate, one of the most weakly attractive known. Its weakness is such that, as experiment shows, a hydrogen fluid does not wet it at low temperature [94], as simulation also show [12]. The second choice namely D =100 K and a =2.05 Å, is roughly in the scope of what one would expect for p-H_2 molecules close to a silica substrate [95]; we thus, henceforth, refer to the scenerio described by this set of parameters as Glass. It should be stressed, however, that in neither case do we aim to accurately reproduce the exact physical interactions (which requires more elaborate functional forms), as that turns out not to matter much in the end, as we show below. Instead, our primary aim is that of investigating opposite ends of the adsorption continuum. The considerably greater well depth and shorter range of its repulsive core, render the "Glass" cavity much more attractive to p-H_2 molecules than the Cs cavity.

4.B Results

4.B.1 Energetics

We set about the illustration of the simulation results by discussing the computed energetics. Fig. 4.1 displays the ground state [96] (i.e., $T = 0$) energy per p-H_2 molecule (in K) as a function of the number of molecules in the cavity. Both curves feature minima at specific number of molecules, which

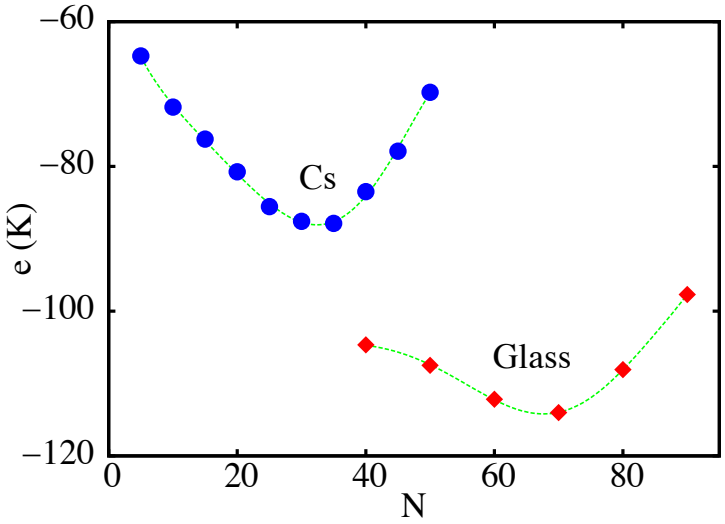

Figure 4.1: Energy per hydrogen molecule e (in K) versus number N in the $T \to 0$ limit, inside a Cs (filled circles) and Glass (diamonds) cavities of radius 10 Å. Dashed lines are fits to the data. Statistical errors are at the most equal to symbol size.

correspond to the minimum number of molecules that fills the cavity, at thermodynamic equilibrium. The curve for glass is shifted some 30 K downward with respect to that for Cs, and its minimum is attained for a value of N close to seventy molecules, over twice as much as the corresponding one for a Cs cavity. This is certainly consistent with the greater adsorption exerted by the Glass cavity, and gives us an idea of the range within which N can vary inside a cavity of this size. An interesting thing to note is that for a Cs cavity, the minimum occurs at an energy close to -88.5 K, identical to the ground state chemical potential (Chapter 2) for solid p-H_2. This implies that a cavity of this size is barely at the wetting threshold for a weakly adsorbing substrate such as Cs.

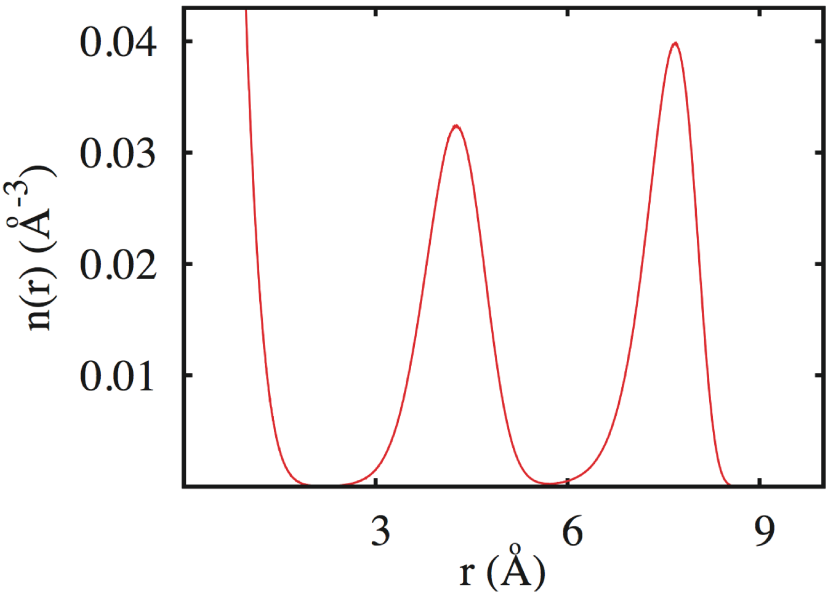

Figure 4.2: Radial density profile $n(r)$ in (Å^{-3}) for 70 p-H_2 molecules inside a Glass cavity at $T = 0.5$ K, modeled as explained in the text. The strong peak at the origin signals the presence of a particle at the center of the cavity. Statistical errors are not visible on the scale of the figure.

4.B.2 Structure of p-H_2 cluster in confinement

Glass cavity

In order to gain insight on the structure of p-H_2 inside the cavity, we examine the computed spherically averaged radial density of molecules $n(r)$, as a function of the distance from the centre of the cavity. Fig. 4.2 shows this quantity at $T = 0.5$ K for the case of seventy molecules inside the Glass cavity. Density profiles for systems of sixty and fifty molecules in the Glass cavity look very similar, the heights of the two peaks shown in Fig. 4.2 being slightly reduced. The density profile shows that molecules are arranged on concentric spherical shells, corresponding to the sharp density peaks. The half width of

these peaks is less than 1 Å, i.e., shells are rigid, molecular excursions in the radial direction being fairly limited. This is true even within the shells, as molecules are scarcely mobile, held in place by the hard core repulsion of the intermolecular potential, which dominates the physics of the system at such dense parking. Consequently, quantum mechanical exchanges of molecules, which underlie the superfluid response in a quantum many-body system of indistinguishable particles, are strongly suppressed, and no appreciable superfluid response is obtained in this case.

Cesium cavity

A very different physical scenario, than in the Glass cavity, takes place in the Cs enclosure, as shown in Fig. 4.3. Solid line shows the density profile for a cluster of 32 molecules, i.e., the minimum of the energy curve in Fig. 4.1, at $T = 1$ K. Also shown (dashed line) is the density profile for the same number of molecules in a Glass cavity. There is a clear difference between the arrangements of the p-H_2 molecules in the various cases; in the Glass cavity, all the molecules are close to the surface, whereas in the Cs one they form two concentric shells, the outer sitting considerably closer to the centre of the cavity, and further away from its surface. This is, obviously, a consequence of the weakness of the Cs substrate compared to the Glass one, and of the consequent greater importance of the role played by the repulsive core of the intermolecular potential at short distances.

Another important feature is that, unlike in the case shown in Fig. 4.2, the demarcation between the two shells present in the Cs cavity is not nearly as sharp as in the glass one, as the density dips but does not go all the way to zero between the two peaks, as in Fig. 4.2. This is indicative of molecular

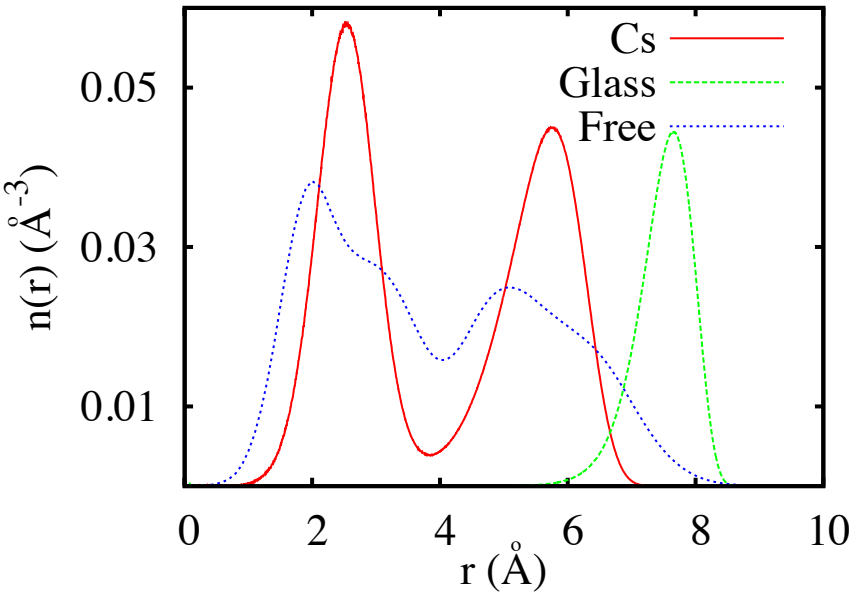

Figure 4.3: Radial density profile $n(r)$ in (Å^{-3}) for 32 p-H_2 molecules inside a Cs cavity (solid line) at $T = 1$ K, modeled as explained in the text. Also shown are the profiles for the same number of molecules inside a Glass cavity (dashed line) and in a free standing p-H_2 cluster (dotted line). Statistical errors are small on the scale of the figure.

delocalization, as well as of the possibility of significant quantum mechanical exchanges and ensuing superfluidity. In this respect, the density profile of 32 p-H_2 molecules in the Cs cavity is closer to that of a free p-H_2 cluster comprising the same number of molecules (also shown in Fig. 4.3, dotted line, computed separately in this work), than to that predicted in the stronger Glass enclosure. The profile of a free standing cluster extends further out as no repulsive cavity wall is present.

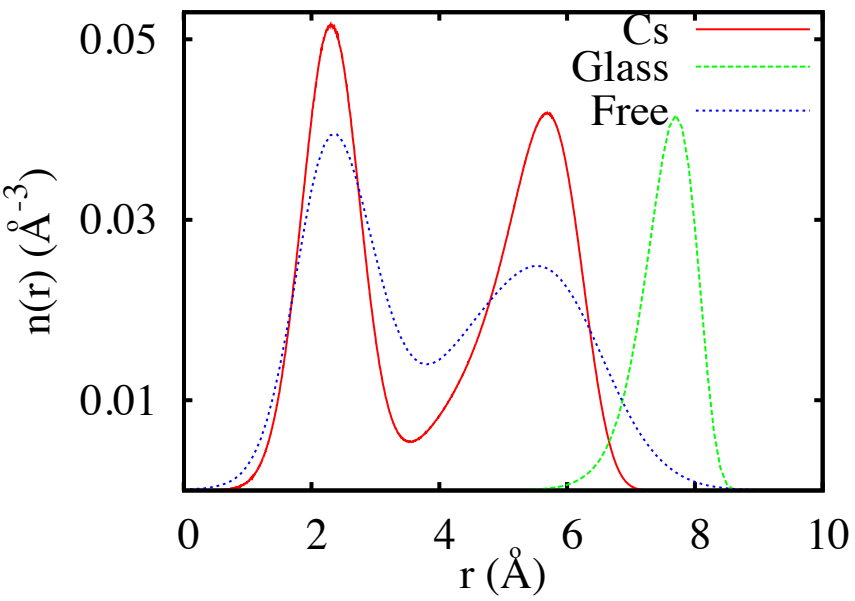

Figure 4.4: Radial density profile $n(r)$ in (Å^{-3}) for 30 p-H_2 molecules inside a Cs cavity (solid line) at $T = 0.5$ K, modeled as explained in the text. Also shown are the profiles for the same number of molecules inside a Glass cavity (dashed line) and in a free standing p-H_2 cluster (dotted line). Statistical errors are not visible on the scale of the figure.

4.B.3 Enhanced superfluid response in cesium cavity

The most important results of this study, however, is that the superfluid response of the cluster which is enclosed in the Cs cavity is greatly enhanced compared to the free ones. For example, in the case of the minimum filling in the Cesium cavity, at $T = 1$ K, corresponding to 32 p-H_2 molecules, the superfluidity of the cluster in the Cs cavity is close to 50%, whereas that of the free cluster at the same temperature is essentially zero (statistical noise level) [97]. In other words, *confinement has the effect of greatly enhancing the*

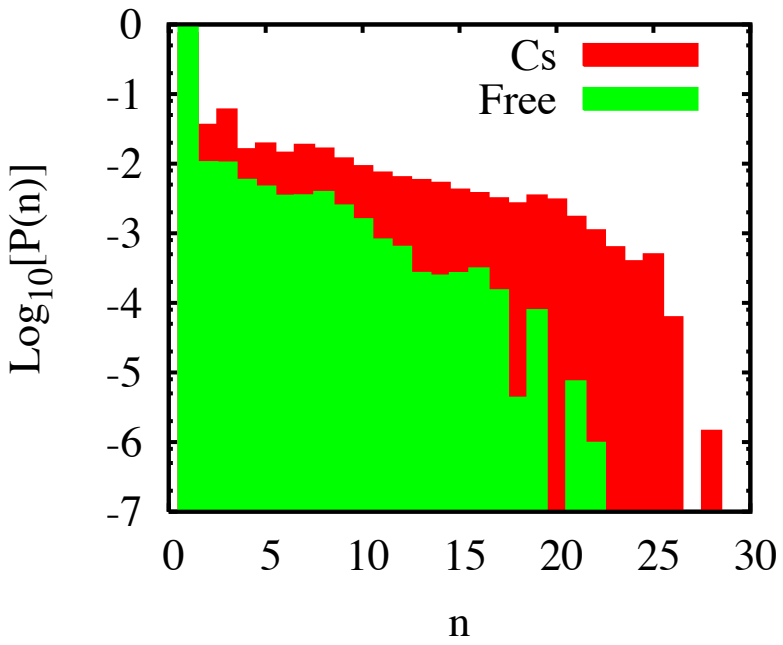

Figure 4.5: Logarithm of the probability of occurrence of permutation cycles of length n (i.e., comprising n p-H_2 molecules) in a cluster of thirty molecules enclosed in a Cs cavity (see text), and in a free cluster, at $T = 0.5$ K. Values lower than $\sim 10^{-4}$ should be regarded as statistical noise.

superfluid response of the p-H_2 cluster. This is confirmed by the occurence of exchange cycles including as many as 25 of the 32 molecules in the Cs cavity enclosed cluster, whereas no cycles comprising more than six molecules are observed in a free cluster. The radial density profile of the free cluster displays considerably more structure in the inner shell, suggesting that molecules are more localized than inside the cavity. Indeed, in the case of 30 p-H_2 molecules, the cluster is 100% superfluid when enclosed in a Cs cavity of radius 10 Å, while the free standing cluster is only 30% superfluid, both at $T = 0.5$ K. Alongside our direct computation of the superfluidity of these clusters in both cases, the radial density profile, Fig. 4.4, and observation of the exchange cycles do lend

further evidence to the enhancement of the superfluid response. Fig. 4.5 is a quantitative comparison of the probability of occurrence of permutation cycles including n molecules ($1 \leq n \leq 30$) in a cluster of 30 p-H_2 molecules enclosed in the Cs cavity, versus in one that is free standing. Indeed, the occurrence of cycles including as many as twenty-five of the thirty molecules is orders of magnitudes more likely in a cluster that is enclosed in the Cs cavity [98]. If the cavity is made much more attractive, as is the case for the Glass one, exchanges are strongly suppressed, as molecules arrange orderly, to form a thin shell near the surface; on the other hand, in a weakly attractive cavity, confinement renders the cluster more compact than in free space, increasing the tendency of molecules to exchange. Thus, the environment experienced by molecules inside the weak Cs cavity is such that the formation of a solid-like cluster, which takes place in free space, is frustrated; the cluster remains liquid-like, as the substrate is not attractive enough to promote crystallization near the surface, which is what happens in strong adsorbents like silica or carbon.

CONCLUSIONS

In this thesis, we presented our simulation results showing that it is possible to dramatically enhance the superfluid response of a system of p-H_2 clusters in nanoscale confinement, if the medium is weakly attractive. Our method has been Path Integral Monte Carlo, implemented using the Continuous-space Worm Algorithm which affords accurate calculation of the low temperature thermodynamics of our system of interest, including (but not limited to) the energetics, structure, momentum distribution and superfluid response.

The size of the cavity for which we presented our results, i.e., 20 Å diameter, seems to offer the right interplay of surface and bulk properties to lead to a novel phase; we also carried out simulations for Cs cavities of diameter 15 and 10 Å, and found equilibrium superfluid clusters of around 17 molecules in the first case, no adsorption in the latter. If the diameter is made greater, bulk physics (i.e., the equilibrium crystalline phase of p-H_2) quickly becomes dominant and the superfluid response is consequently suppressed.

Our study also has massive implications on the possible observation of the yet elusive bulk superfluid phase of p-H_2. The first thing that we need to assess, is the dependence of our results on the specific choice of geometry adopted in this study, namely that of a spherical cavity. With respect to this, it is important to note that the main physical effects observed in this work, that

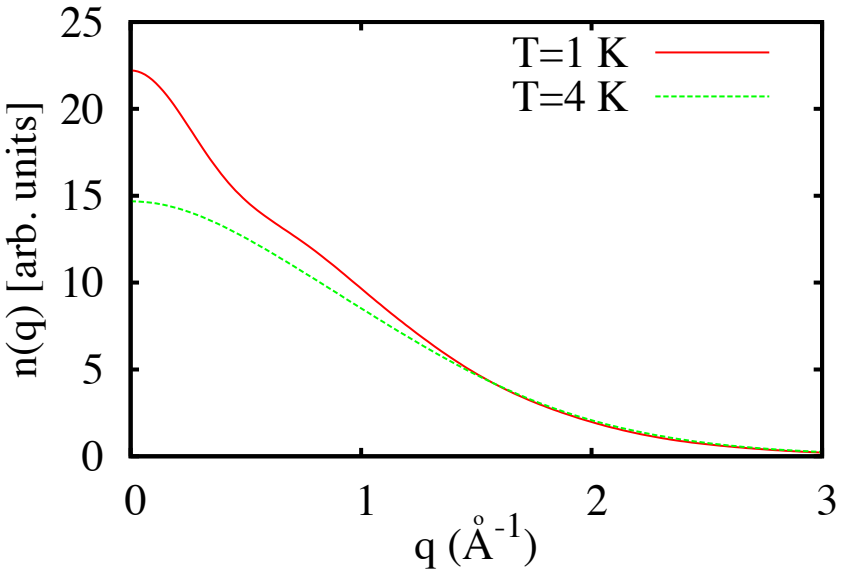

Figure 4.6: Momentum distribution for a system of 32 p-H_2 molecules inside a Cs cavity of radius 10 Å at T=4 K and T=1 K.

leads to the enhancement of intermolecular quantum exchanges, hinges on the weakness of the substrate and on the characteristic size of the confining region. Thus, we predict that it should also take place in different geometries (e.g., cylindrical), with a comparable confining length (e.g., diameter). Hence, the issue of experimentally observing this predicted superfluid response of p-H_2 is centred on creating an adsorbing porous matrix, whose microscopic structure consists of interconnected nanoscale size pores, through which superflow could be established, at a temperature of the order of a fraction of a K.

While coating the walls of a porous glass with relatively thick (a few layers) film of Cs or Rb, for example, may not be experimentally feasible at this time, perhaps techniques such as those utilized to fabricate nanoholes semiconductor membranes, presently utilized to investigate the hydrodynamics of superfluid helium in quasi-one-dimension [99] could be adopted. As a final remark, we

mention that one might also think of detecting a superfluid transition of the embedded p-H_2 fluid by measuring the momentum distribution, typically by neutron scattering [25], and looking for the appearance at low temperature of a peak at zero momentum [25], which signals the onset of Bose-Einstein condensation, intimately connected to superfluidity. This requires no actual bulk superflow, nor the use of molecular probes, which renders the unambiguous detection of superfluidity problematic in free standing clusters [30]. While the peak is not sharp as it would be in bulk superfluid, but rather broadened by the fact that the system is confined over a length of $\sim$1 nm, its detection should still be possible, as is well depicted in Fig. 4.6.

Bibliography

[1] D. R. Tilley & J. Tilley, John Wiley & Sons Inc, New York, 1974.

[2] van Delft D 2007 (Amsterdam: Edita KNAW).

[3] P. Kapitza, *Nature* **74**, 141 (1938).

[4] J. F. Allen and A. D. Misener, *Nature* **75**, 141 (1938).

[5] L. Tisza, *Nature* **141**, 913 (1938).

[6] See, for instance, A. Leggett, *Quantum Liquids*, (Oxford University Press, New York, 2006).

[7] See, for instance, R. P. Feynman, *Statistical Mechanics* (Addison-Wesley, New York, 1972).

[8] D. M. Ceperley, Rev. Mod. Phys. **67**, 279 (1995).

[9] See, for instance, M. Boninsegni and N. Prokof'ev, Rev. Mod. Phys. **84**, 759 (2012).

[10] Ginzburg, V. L. & Sobyanin, A. A. *JETP Lett.* **15**, 242 (1972).

[11] Boninsegni, M. *Phys. Rev. Lett.* **111**, 235303 (2013).

[12] M. Boninsegni, *Phys. Rev. B* **70**, 125405 (2004).

[13] M. Wagner & D.M. Ceperly, *J. Low Temp. Phys.* **102**, 275 (1996).

[14] K. Nho & E. Manousakis, *Phys. Rev. B* **65**, 115409 (2002).

[15] Joseph Turnbull, Doctoral Thesis, University of Alberta (2008).

[16] M. C. Gordillo & D.M. Ceperly, *Phys. Rev. Lett.* **79**, 3010 (1997).

[17] M. Boninsegni, *New J. Phys.* **7**, 78 (2005).

[18] G. M. Seidel, H. J. Maris, F. I. B. Williams, and J. G. Cardon. *Phys. Rev. Lett.* **56**, 2380 (1986).

[19] H. J. Maris, G. M. Seidel, and F. I. B. Williams. *Phys. Rev. B* **36**, 6799 (1987).

[20] Tell, J. L. & Maris, H. J. *Phys. Rev. B* **28**, 5122 (1983).

[21] Molz, E., Wong, A., Chan, M. H. W., & Beamish, J. R. *Phys. Rev. B* **48**, 5741 (1993).

[22] Mason, G. *Proceedings of the Royal Society A: Mathematical, Physical and Engineering Sciences* **415**, 453 (1988).

[23] Bretz, M. & Thomson, A. L. *Phys. Rev. B* **24**, 467 (1981).

[24] M. Schindler, A. Dertinger, Y. Kondo, and F. Pobell *Phys. Rev. B* **53**, 11451 (1996).

[25] Sokol, P. E., Azuah, R. T., Gibbs, M. R., & Bennington, S. M. *J. Low Temp. Phys.* **103**, 23 (1996).

[26] Chan, M. H. W., Blum, K. I., Murphy, S. Q., Wong, G. K. S., & Reppy, J. D. *Phys. Rev. Lett.* **61**, 1950 (1988).

[27] Mezzacapo, F., & Boninsegni, M. *Phys. Rev. A* **75**, 033201 (2007).

[28] P. Sindzingre, D.M. Ceperly, and M.L. Klein, *Phys. Rev. Lett.* **67**, 1871 (1991).

[29] Kwon, Y., & Whaley, K. B. *Phys. Rev. Lett.* **89**, 273401 (2002).

[30] S.Grebenev, B. Sartakov, J.P. Toennies, & A.F. Vilesov, *Science* **289**, 1532 (2000).

[31] See, for instance, Callegari, C., Lehmann, K. K., Schmied, R., & Scoles, G. *J. Chem. Phys.* **115**, 10090 (2001).

[32] Mezzacapo, F., & Boninsegni, M. *Phys. Rev. E* **97**, 045301 (2006).

[33] Ross, D., Taborek, P., & Rutledge, J. *Phys. Rev. B* **58**, 4274 (1998).

[34] I. F. Sivera & V. V. Goldman, *J. Chem. Phys.* **69**, 4209 (1978).

[35] Omiyinka, T., & Boninsegni, M. *Phys. Rev. B* **88**, 024112 (2013).

[36] Kim, H.-Y., Gatica, S. M., & Cole, M. W. *J. Phys. Chem. A* **111**, 12439 (2007).

[37] The same argument justifies the neglect of surface defects and corrugation, an assumption routinely made in numerical studies of adsorption of He or p-H_2 on alkali substrates. See, for instance, Ref. [12].

[38] Del Maestro, A., Boninsegni, M., & Affleck, I. *Phys. Rev. Lett.* **106**, 105303 (2011).

[39] Chui, S. *Phys. Rev. B* **43**, 11523 (1991).

[40] Jain, P., Cinti, F., & Boninsegni, M. *Phys. Rev. B* **84**, 014534 (2011).

[41] Boninsegni, M., Prokof'ev N., & Svistunov, B. *Phys. Rev. Lett.* **96**, 070601 (2006).

[42] Boninsegni, M., Prokof'ev N., & Svistunov, B. *Phys. Rev. E* **74**, 036701 (2006).

[43] R. P. Feynman. *Rev. Mod. Phys* **20**, 348 (1948).

[44] N. Metropolis, N. Rosenbluth, A. W. Rosenbluth, A. H. Teller and E. Teller, J. Chem. Phys. **21**, (1953) 1087-1092.

[45] See Ref. [48]

[46] Feynman & Hibbs, *Quantum Mechanics and path integrals*, McGraw-Hills, 1967

[47] Boninsegni M. *Journal of Low Temperature Physics* **141**, 112 (2005).

[48] D.M. Ceperly, *Rev. Mod. Phys.* **67**, 279 (1995).

[49] Fabio Mezzacapo, *Structure, Superfluidity and Quantum Melting of Hydrogen Clusters: A Quantum Monte Carlo Study*, Doctoral Thesis, University of Alberta (2008).

[50] M. Boninsegni, *Phys. Rev. B* **79**, 174203 (2009).

[51] S. Jang, S. Jang, and G. A. Voth, *J. Chem Phys.* **115**, 7832 (2001).

[52] P. Sindzingre, M. L. Klein, and D. M. Ceperly, *Phys. Rev. Lett.* **63**, 1601 (1989).

[53] Colin Morningstar, *The Monte Carlo Method in Quantum Mechanics*, Carnegie Mellon University.

[54] H. Flyvbjerg & H. G. Petersen, Error estimates on averages of correlated data, *J. Chem. Phys.* **91**, 461 (1989).

[55] M. J. Norman, R. O. Watts and U. Buck, *J. Chem. Phys.* **81**, 3500 (1984).

[56] M. Moraldi, *J. Low Temp. Phys.* **168**, 275 (2012).

[57] R. J. Hemley and H.-K. Mao, *J. Low Temp. Phys.* **122**, 331 (2001).

[58] J. Kohanoff, *J. Low Temp. Phys.* **122**, 297 (2001), and references therein.

[59] N. W. Ashcroft in *Proceedings of the International School of Physics "Enrico Fermi," Course CXLVII, High pressure Phenomena*, edited by R. J. Hemley, G. L. Chiarotti, M. Bernasconi, and L. Ulivi (IOS, Amsterdam, 2002), p. 151.

[60] M. W. C. Dharma-wardana and F. Perrot, *Phys. Rev. A* **26**, 2096 (1982).

[61] T. W. Barbee, M. L. Coehn and J. L. Martins, *Phys. Rev. Lett.* **62**, 1150 (1989).

[62] D. Hohl, V. Natoli, D. M. Ceperley and R. M. Martin, *Phys. Rev. Lett.* **71**, 541 (1993).

[63] J. Kohanoff, S. Scandolo, G. L. Chiarotti and E. Tosatti, *Phys. Rev. Lett.* **78**, 2783 (1997).

[64] H. Kitamura, S. Tsuneyuki, T. Ogitsu and T. Miyake, *Nature Physics* **404**, 259 (2000).

[65] C. J. Pickard and R. J. Needs, *Nature Physics* **3**, 473 (2007).

[66] D. M. Ceperley and B. J. Alder, *Phys. Rev. B* **36**, 2092 (1987).

[67] V. Natoli, R. M. Martin and D. M. Ceperley, *Phys. Rev. Lett.* **70**, 1952 (1993).

[68] C. Pierleoni, D. M. Ceperley, B. Bernu, W. R. Magro, *Phys. Rev. Lett.* **73**, 2145 (1994).

[69] W. R. Magro, D. M. Ceperley, C. Pierleoni and B. Bernu, *Phys. Rev. Lett.* **76**, 1240 (1996).

[70] C. Pierleoni, D. M. Ceperley and M. Holzmann, *Phys. Rev. Lett.* **93**, 146402 (2004).

[71] K. T. Delaney, C. Pierleoni and D. M. Ceperley, *Phys. Rev. Lett.* **97**, 235702 (2006).

[72] F. Operetto & F. Pederiva, *Phys. Rev. B* **73**, 184124 (2006).

[73] U. Buck, F. Huisken, A. Kohlhase, D. Otten, and J. Schaeffer, *J. Chem. Phys.* **78**, 4439 (1983).

[74] For a comparison of the Silvera-Goldman and Buck potentials, see, for instance, E. Cheng and K. B. Whaley, *J. Chem. Phys.* **104**, 3155 (1996).

[75] M. Boninsegni, C. Pierleoni and D. M. Ceperley, *Phys. Rev. Lett.* **72**, 1854 (1994).

[76] S. Moroni, F. Pederiva, S. Fantoni and M. Boninsegni, *Phys. Rev. Lett.* **84**, 2650 (2000).

[77] S.-Y. Chang and M. Boninsegni, *J. Chem. Phys.* **115**, 2629 (2001).

[78] M. Takahashi and M. Imada, *J. Phys. Soc. Jpn.* **53**, 3871 (1984).

[79] At the highest density considered here, the estimated correction to the computed pressure arising from the tail of the intermolecular potential has a magnitude worth approximately 3% of the total pressure.

[80] See Ref. [32]

[81] See Ref. [50]

[82] F. Simon, Z. Phys. **15**, 307 (1923).

[83] J. Stewart, *J. Chem. Phys. Solids* **1**, 146 (1956).

[84] O. Schnepp, *Phys. Rev. A* **2**, 2574 (1970).

[85] A. Driessen, J. A. de Waal and I. F. Silvera, *J. Low Temp. Phys.* **34**, 255 (1979).

[86] Y. A. Freiman, A. Grechnev, S. M. Tretyak, A. F. Goncharov and R. J. Hemley, *Phys. Rev. B* **86**, 014111 (2012).

[87] P. Loubeyre, R. LeToullec, D. Hausermann, M. Hanfland, R. J. Hemley, H.-K. Mao, & L. W. Finger, *Nature (London)* **383**, 702 (1996).

[88] Y. Akahama, M. Nishimura, H. Kawamura, N. Hirao, Y. Ohishi and K. Takemura, *Phys. Rev. B* **82**, 060101(R) (2010).

[89] H.-K. Mao and R. J. Hemley, *Rev. Mod. Phys.* **66**, 671 (1994).

[90] P. Vinet, J. Ferrante, J. H. Rose and J. R. Smith, *J. Geophys. Res.* **92**, 9319 (1987).

[91] H. E. Lorenzana, I. F. Silvera and K. A. Goettel, *Phys. Rev. Lett.* **64**, 1939 (1990).

[92] See, for instance, R. T. Azuah, W. G. Stirling, H. R. Glyde, M. Boninsegni, P. E. Sokol and S. M. Bennington, *Phys. Rev. B* **56**, 14620 (1997).

[93] Chizmeshya, A., Cole, M. W., & Zaremba, E. *J. Low Temp. Phys.* **110**, 677 (1998).

[94] See Ref. [33].

[95] The values D=100 K and a=2.05 Å have been utilized in some studies to characterize the interaction of a helium atom with a Glass substrate. See, for instance, L. Pricaupenko and J. Treiner, Phys. Rev. Lett. **74**, 430 (1995). For p-H_2 one might expect D to be as much as twice as large, while a could be greater by approximately 10%, based on the simple Loretz-Berthelot mixing rule.

[96] We obtain ground state estimates by extrapolating to $T = 0$ low temperature results. In pratice, we find that energy values, as well as radial density profiles, remain unchanged, on the scales of the figures shown here, below $T \lesssim 4$ K.

[97] The value of the superfluid fraction is directly computed by simulation using the well-known "area" estimator. See, P. Sindzingre, M. L. Klein and D. M. Ceperley, Phys. Rev. Lett. **63**, 1601 (1989).

[98] The probability distributions shown in Fig. 4.5 have only illustrative purpose. There is no known way of extracting from them the value of the superfluid fraction, which is directly computed by simulation using the "area" estimator, as mentioned above.

[99] See, for instance, M. Savard, G. Dauphinais, and G. Gervais, Phys. Rev. Lett. **107**, 254501 (2011).